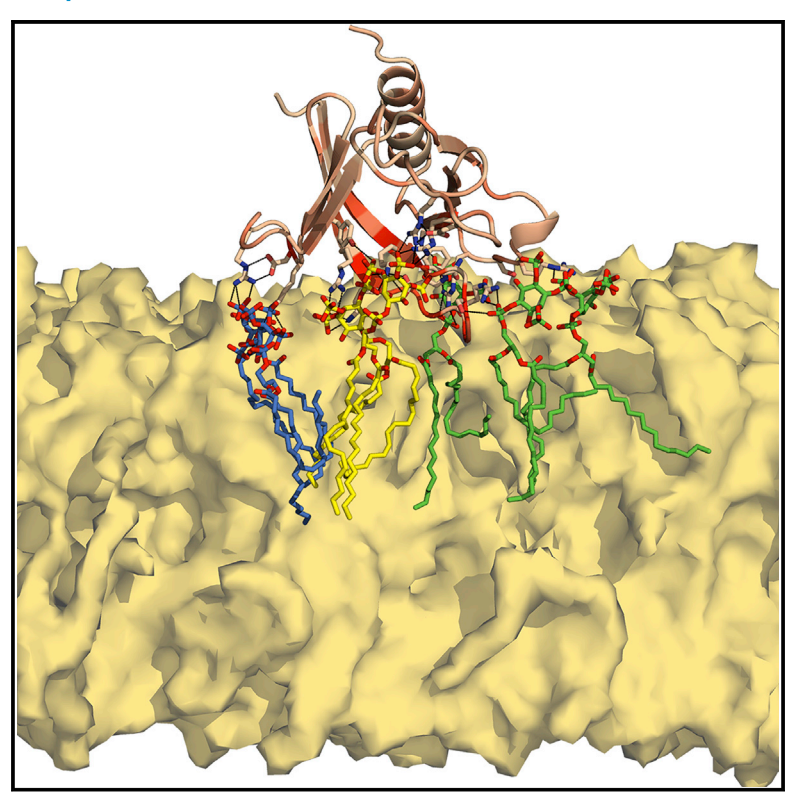
# Structural basis for the association of PLEKHA7 with membrane-embedded phosphatidylinositol lipids

#### **Graphical abstract**



#### **Authors**

Alexander E. Aleshin, Yong Yao, Amer Iftikhar, ..., Wonpil Im, Garth Powis, Francesca M. Marassi

#### Correspondence

fmarassi@sbp.edu

#### In brief

The interactions of PLEKHA7 with membrane-bound phosphatidylinositol (PIP) lipids are critical for cell signaling and cytoskeletal organization. Here, we describe the structural basis for PIP recognition by its PH domain and provide a roadmap for understanding how this contributes to the functions of PLEKHA7.

#### **Highlights**

- The structure of the PLEHA7 PH domain reveals multiple binding sites for PIP lipids
- The PH domain contains major elements of PIP recognition by PLEKHA7
- The membrane scaffold promotes multivalent association of one PH domain with PIPs
- The PLEKHA7 PH domain induces membrane PIP clustering







#### **Article**

# Structural basis for the association of PLEKHA7 with membrane-embedded phosphatidylinositol lipids

Alexander E. Aleshin, 1,3 Yong Yao, 1,3 Amer Iftikhar, 2 Andrey A. Bobkov, 1 Jinghua Yu, 1 Gregory Cadwell, 1 Michael G. Klein, 1 Chuqiao Dong, 2 Laurie A. Bankston, 1 Robert C. Liddington, 1 Wonpil Im, 2 Garth Powis, 1 and Francesca M. Marassi 1,4,\*

#### **SUMMARY**

PLEKHA7 (pleckstrin homology domain containing family A member 7) plays key roles in intracellular signaling, cytoskeletal organization, and cell adhesion, and is associated with multiple human cancers. The interactions of its pleckstrin homology (PH) domain with membrane phosphatidyl-inositol-phosphate (PIP) lipids are critical for proper cellular localization and function, but little is known about how PLEKHA7 and other PH domains interact with membrane-embedded PIPs. Here we describe the structural basis for recognition of membrane-bound PIPs by PLEHA7. Using X-ray crystallography, nuclear magnetic resonance, molecular dynamics simulations, and isothermal titration calorimetry, we show that the interaction of PLE-KHA7 with PIPs is multivalent, distinct from a discrete one-to-one interaction, and induces PIP clustering. Our findings reveal a central role of the membrane assembly in mediating protein-PIP association and provide a roadmap for understanding how the PH domain contributes to the signaling, adhesion, and nanoclustering functions of PLEKHA7.

#### **INTRODUCTION**

PLEKHA7 (pleckstrin homology domain containing family A member 7) is a major component of the cytoplasmic region of epithelial adherens junctions that functions to ensure cell-cell adhesion and tight junction integrity through its interactions with cytoskeleton proteins (Meng et al., 2008; Paschoud et al., 2014; Pulimeno et al., 2010; Rouaud et al., 2020). Increased levels of human PLEKHA7 are associated with hypertension (Levy et al., 2009) and glaucoma (Awadalla et al., 2013), and PLEKHA7 protein staining has been reported in several human cancers, including advanced breast, renal, and ovarian cancer (Kourtidis et al., 2015; Tille et al., 2015), with highest occurrences in colon cancer (Castellana et al., 2012). A recent study (Nair-Menon et al., 2020) showed that disruption of the apical junction localization of RNA interference machinery proteins correlates with loss of PLEKHA7 in human colon tumors and poorly differentiated co-Ion cancer cell lines, while restoration of PLEKHA7 expression restores proper localization of RNA interference components and suppresses cancer cell growth in vitro and in vivo. Moreover, we have observed (Jeung et al., 2011) that PLEKHA7 associates with proteins of the membrane-bound KRAS (Kirsten rat sarcoma viral oncogene homolog) signaling nanocluster in colon cancer cells, and that plekha7 gene knockdown inhibits the proliferation of colon cancer cells with mutated KRAS, but not normal cells with wild-type KRAS. PLEKHA7, therefore, represents an attractive druggable target for the selective inhibition of signaling and its tumor-related functions in colorectal cancer. Despite its importance, the molecular basis for the role of PLEKHA7 in these disorders is poorly understood.

The 1,271-residue PLEKHA7 is one of nine family members characterized by a 120-residue N-terminal pleckstrin homology (PH) domain (Figure S1A). PH domains are found in more than 100 different proteins. They are known for their ability to bind phosphatidyl-inositol-phosphate (PIP) lipids within cell membranes, and their association with PIPs is essential for intracellular signaling, cytoskeletal organization, and the regulation of intracellular membrane transport (DiNitto and Lambright, 2006; Lemmon, 2007). Notably, PH domains can be selectively targeted by small molecules that inhibit their signaling function (Indarte et al., 2019; Meuillet et al., 2003, 2010). In the case of PLEKHA7, the PH domain is required for establishing proper subcellular localization through its interactions with PIPs (Wythe et al., 2011), and thus could offer a new avenue for attacking cancer by inhibiting PLEKHA7 localization.

Following the first nuclear magnetic resonance (NMR) structures of pleckstrin (Yoon et al., 1994) and  $\beta$ -spectrin (Macias et al., 1994), the structures of many other PH domains have



<sup>&</sup>lt;sup>1</sup>Cancer Center, Sanford Burnham Prebys Medical Discovery Institute, 10901 North Torrey Pines Road, La Jolla, CA 92037, USA

<sup>&</sup>lt;sup>2</sup>Departments of Biological Sciences, Chemistry and Bioengineering, Lehigh University, Bethlehem, PA 18015, USA

<sup>&</sup>lt;sup>3</sup>These authors contributed equally

<sup>&</sup>lt;sup>4</sup>Lead contact

<sup>\*</sup>Correspondence: fmarassi@sbp.edu https://doi.org/10.1016/j.str.2021.03.018





been reported, either in their free state or complexed with soluble inositol phosphate (IP) small molecules (Moravcevic et al., 2012). These have provided important functional insights, but little is still known about the way in which PH domains associate with full-length PIPs incorporated in membranes, and nothing is known about the structural basis for PIP binding by PLEKHA7. Using a multidisciplinary approach that combined X-ray crystallography, NMR, all-atom molecular dynamics (MD) simulations, and isothermal titration calorimetry (ITC) binding measurements, we have determined the structures of the PLEHA7 PH domain and characterized its interactions with membrane-embedded PIPs with atomic-level detail. The data reveal three PLEKHA7 binding sites for PIP, and demonstrate that confinement of PIP molecules by the membrane assembly is important for promoting the multivalent association of one PH domain with multiple PIPs leading to membrane surface localization.

#### **RESULTS AND DISCUSSION**

#### Structure of the PLEKHA7 PH domain

We obtained crystals for two states of the PH domain of PLE-KHA7 — one ligand-free (PHA7 $_{\rm APO}$ ) and the other bound to sulfate from the crystallization buffer (PHA7<sub>S</sub>)-and determined two structures, which refined to 2.80-Å and 1.45-Å resolution, respectively (Figures 1A, 1B, S1C, and S1D; Table S1). Each structure crystallized in a different space group and has two copies of the protein per crystallographic asymmetric unit, but the protein-protein interfaces differ in each case and do not appear to reflect biologically functional dimers. PLEKHA7 adopts the PH domain signature fold (Lemmon, 2007; Lietzke et al., 2000): a seven-stranded β barrel, capped at one end by a 16-residue  $\alpha$  helix. The barrel opening is highly positively charged and lined by the  $\beta1-\beta2$ ,  $\beta3-\beta4$ , and  $\beta6-\beta7$  loops, which are hypervariable in both length and sequence across the PH domain family. The K173-K183-R185 motif, at the end of B1 and start of  $\beta 2$ , forms the canonical IP binding site of PH domains (Moravcevic et al., 2012). In the case of PHA7<sub>S</sub>, this site-denoted here as site I-is occupied by one of two sulfate anions resolved in the structure. No electron density was observed for either the β6-β7 loop or C-terminal residues S285-R298, which were included in the sequence of PHA7<sub>S</sub> (residues 164-298) but deleted in PHA7<sub>APO</sub> (residues 164-285). The structures show that the PH domain is confined to residues 164-285, and subsequent NMR, ITC, and MD simulation studies utilized this trimmed sequence, henceforth referred to as PHA7 (Figure S1B).

To further examine the protein conformation and dynamics in solution, we prepared  $^{15}\text{N}/^{13}\text{C}$  labeled PHA7 for NMR experiments. The assigned NMR chemical shifts ( $^{1}\text{HN}$ ,  $^{15}\text{N}$ ,  $^{13}\text{CA}$ , and  $^{13}\text{CB}$ ) show that the protein adopts the same structure in solution as in its crystalline form, and that the long  $\beta6-\beta7$  loop forms a random coil (Figure 1D). The  $^{1}\text{H}/^{15}\text{N}$  nuclear Overhauser effect (NOE) data show that the  $\beta$  strands and helices ( $\alpha1$ ,  $\alpha'$ ) all have similar (>0.8) NOE intensities, consistent with uniform backbone dynamics and conformational order (Figure 1E). By contrast, the termini and loops have distinctly lower NOE intensities, and hence greater extents of dynamics and lower conformational order. High flexibility is observed for  $\beta6-\beta7$  where the intensities approach zero, and also for  $\beta1-\beta2$  and  $\beta3-\beta4$ , loops that are

important for defining the recognition of specific PIP phosphorylation states by other PH domains (Lemmon, 2007).

PLEKHA7 shares 50%–75% amino acid sequence identity with the other PLEKHA family members (Figure S1F), but it is unique in containing a 20-residue insertion between  $\beta 6$  and  $\beta 7$ . Long  $\beta 6-\beta 7$  loops are found in other members of the larger PH domain superfamily. In GRP1 and ARNO (Cronin et al., 2004; Lietzke et al., 2000), the  $\beta 6-\beta 7$  loop forms a  $\beta$  hairpin that elongates the  $\beta$  barrel, generating a more extensive pocket for binding IP, while in the case of ANLN the loop does not appear to be involved in IP binding. The  $\beta 6-\beta 7$  sequence of PHA7 differs from those of GRP1, ARNO, and ANLN.

#### Interactions with soluble IP headgroups and membraneembedded PIPs

To assess the affinity of PHA7 for membrane-embedded PIP lipids, we performed co-sedimentation experiments with PIPcontaining liposomes. While PHA7 does not sediment with pure dipalmitoyl-phosphatidylcholine (diC16-PC) liposomes, incubation with liposomes containing 10% molar diC16-PI(3,4,5) P<sub>3</sub> resulted in abundant co-sedimentation (Figure 2A). Notwithstanding this evident high affinity for PIP-rich membranes, our attempts to co-crystallize PHA7 with either short-chain PIP lipids or soluble IP headgroups—inositol(1,4,5)triphosphate (IP(4,5) P<sub>2</sub>), inositol(1,3,4)triphosphate (IP(3,4)P<sub>2</sub>), or inositol(1,3,4,5)tetraphosphate (IP(3,4,5)P<sub>3</sub>)—resulted in the apo form of the protein, without bound ligand, regardless of crystallization or soaking conditions. This is in line with the micromolar-range dissociation constants (KD) that we measured by ITC for the interaction of PHA7 with soluble IPs (Figure 2B and Table 1). The combined data indicate that PHA7 has modest affinity for soluble IPs but appreciably higher affinity for PIP lipids incorporated in membranes. A similar effect has been reported for the PH domain of kindlin 3, whose binding affinity for PIP was enhanced 1,000-fold upon PIP incorporation in nanodiscs (Ni et al., 2017).

To analyze this effect quantitatively, we performed ITC experiments with PHA7 and PIP-enriched lipid nanodiscs—nanometer-size discoidal membranes that are stabilized by two copies of a membrane scaffold protein derived from the apolipoprotein ApoA1 (Bayburt et al., 2002). We prepared nanodiscs with either pure diC16-PC or a 1:9 molar mixture of diC16-PIP and diC16-PC. Remarkably, the ITC binding affinity measured by titrating the protein with PIP nanodiscs is enhanced by more than one order of magnitude relative to soluble IP headgroups (Figure 2C and Table 1), in line with the co-sedimentation results. Moreover, PHA7 now appears to display some—albeit modest—selectivity (p < 0.05) for phosphatidylinositol(4,5) diphosphate (PI(4,5)P<sub>2</sub>) > phosphatidylinositol(3,4)diphosphate (PI(3,4,P<sub>2</sub>) > phosphatidylinositol(3,4,5)triphosphate (PI(3,4,5) P<sub>3</sub>) lipid membranes.

The simplified nanodisc platform, while powerful, prohibits analysis of binding stoichiometry, because the potential for lipid clustering (Wen et al., 2018) during the nanodisc preparation process makes it challenging to control the composition of individual nanodiscs. Nevertheless, the enhanced affinity for membrane-incorporated PIPs suggests that additional factors—beyond a pure one-to-one PHA7-to-IP headgroup interaction—play a role in recruiting the protein to the membrane surface. The

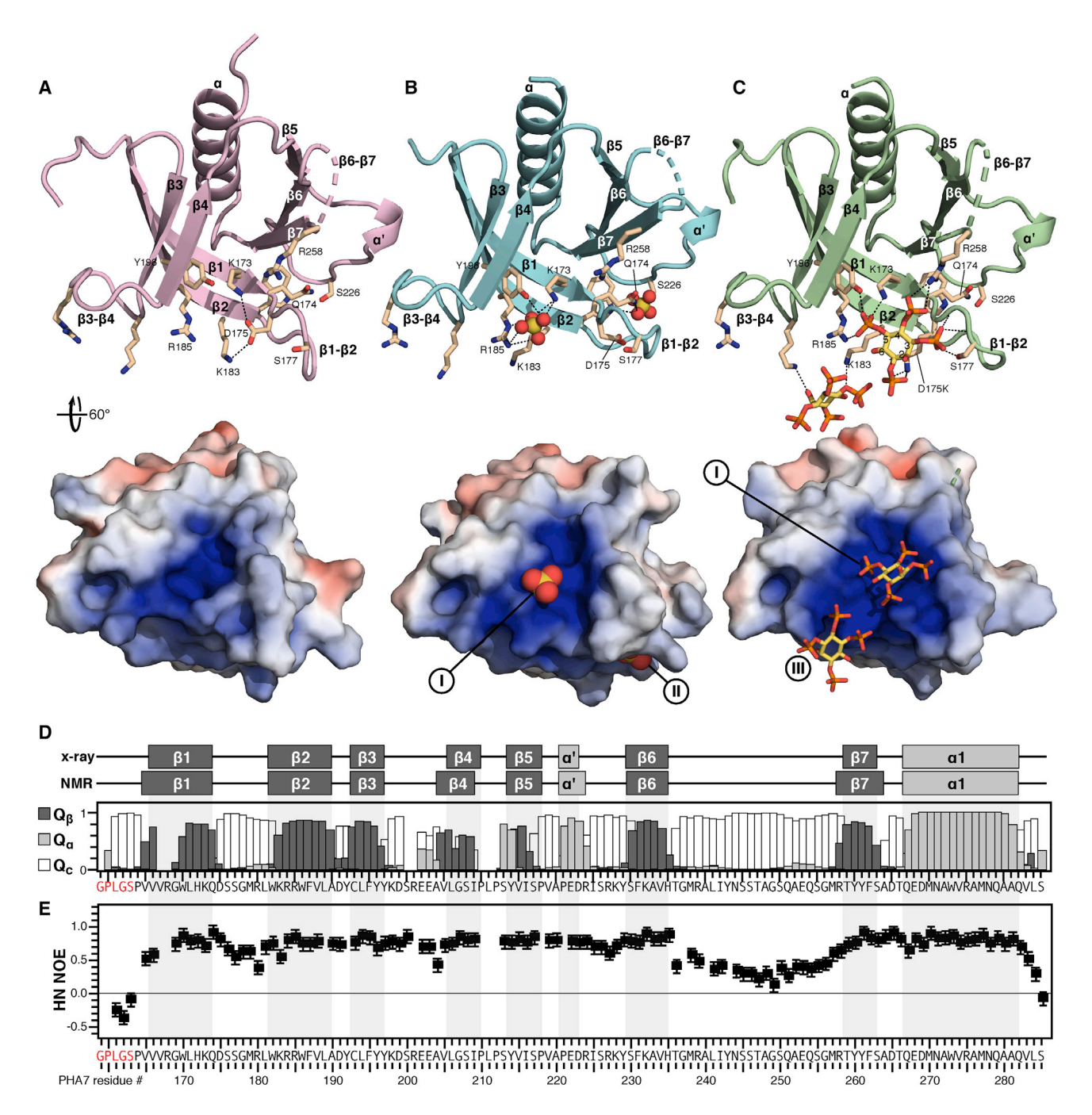


Figure 1. Structure of the PLEKHA7 PH domain

(A) PHA7<sub>APO</sub>.

(B) PHA7<sub>S</sub> bound to sulfate (yellow/orange spheres).

(C) Mutant PHA7-D175K bound to soluble IP(3,4,5)P3 (yellow/orange sticks). Key residues are shown as sticks. Dashes denote protein-protein, protein-sulfate, or protein-IP(3,4,5)P<sub>3</sub> polar contacts (<4 Å). The 60° surface representations are colored by electrostatic potential from -5 kT/e (red) to +5 kT/e (blue). The positions of the three binding sites (I-III) for sulfate or phosphate are marked.

(D and E) Structure and dynamics of PHA7 (164-285) derived from NMR. (D) The secondary structure was derived from TALOS chemical-shift analysis. Bars depict the accuracy (Q) of prediction for  $\alpha$  helix (Q<sub>n</sub>),  $\beta$  strand (Q<sub>n</sub>), or random coil (Q<sub>c</sub>). Elements of the secondary structure derived from crystallography and NMR are depicted above the plot. (E) The heteronuclear <sup>1</sup>H/<sup>15</sup>N NOE relative intensities reflect dynamics of PHA7<sub>APO</sub>. Error bars reflect experimental uncertainty.



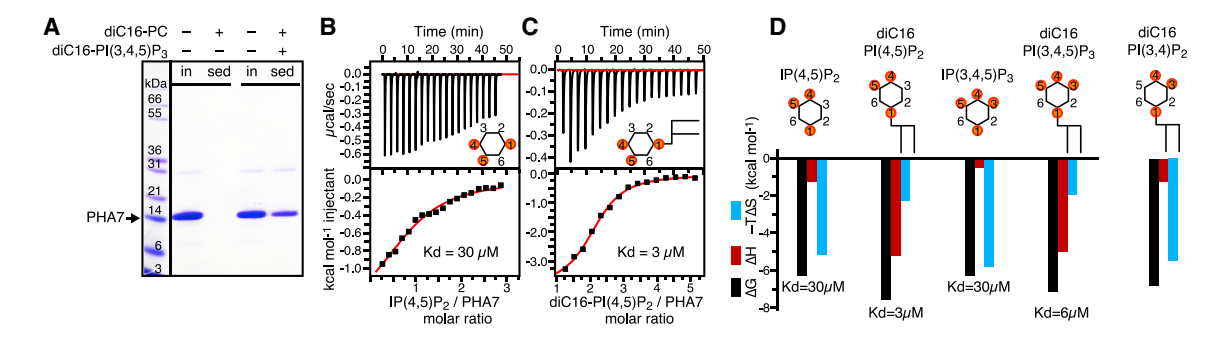


Figure 2. Interactions of PHA7 with PIP lipids and soluble IPs

(A) SDS-PAGE analysis of PHA7 co-sedimentation with diC16-PC liposomes prepared with or without 10% molar diC16-PI(3,4,5)P<sub>3</sub>. Monomeric PHA7 (arrow) migrates with apparent molecular weight of ~15 kDa.

(B–D) Representative ITC binding isotherms (B and C) and free energies (D) measured for titrations of PHA7 with soluble IP(4,5)P<sub>2</sub> and IP(3,4,5)P<sub>3</sub>, or nanodiscs containing 10% molar diC16-PI(4,5)P<sub>2</sub> and diC16-PI(3,4,5)P<sub>3</sub>. Continuous red lines are the best fits of the data to a single-site binding model, used to extract the values of the dissociation constant (Kd).

binding free energies derived from ITC offer some insights in this regard (Figure 2D). The association of PHA7 with free IPs is highly entropy driven, with binding thermodynamics characterized by very small values of favorable enthalpy ( $\Delta$ H) and a much greater entropic component ( $\Delta$ S). The situation is reversed for the association of PHA7 with membrane-embedded PIPs, where the enthalpic component dominates.

We propose that this effect reflects the interaction of one PHA7 molecule with multiple PIP molecules incorporated in the nanodisc membrane, and a reduction of PHA7 and PIP conformational, rotational, and translational degrees of freedom imposed by the membrane scaffold. According to the principles of binding free energy additivity (Jencks, 1981), the observed binding free energy is the sum of the intrinsic binding free energies of the individual ligands plus a "connection" energy-a largely entropic term that reflects the change in the probability of binding due to the change in translational and rotational degrees of freedom that result from connecting the ligands. Such superadditivity is well known in drug development, where chemical linking of weakly binding fragments results in molecules with binding free energy greater than the sum of the individual fragments. In the case of the PHA7-PIP membrane complex, membrane confinement replaces chemical linking, and the additional Jencks "connection" free energy may be attributed to a change in the probability of binding that results from confinement of multiple PIPs and bound PHA7 by the membrane, resulting in overall enhanced affinity. Additional factors such as interactions of the protein with the hydrophobic acyl chains of the lipids may further contribute to the enhanced affinity.

#### Structural basis for binding soluble IPs

In the absence of co-crystals, the structure of PHA7<sub>S</sub> provides useful insights about the protein's interactions with the IP moiety. In PHA7<sub>S</sub> (Figures 1B and S2A) one sulfate anion occupies site I, where it is coordinated by the side chains of K173 in  $\beta1$ , R185 in  $\beta2$ , and Y196 at the end of  $\beta3$ . A second sulfate anion binds on the opposite side of the  $\beta1$ - $\beta2$  loop—denoted here as site II—where it is coordinated by the side chains of Q174 and W182, which define the start and the end of the  $\beta1$ - $\beta2$  loop, and S226 in the middle of the  $\beta5$ - $\beta6$  loop. While IP binding at this second site is considered

"atypical" and thought to occur only in PH domains that lack the canonical binding site (Moravcevic et al., 2012), it has been observed experimentally for the PH domains of spectrin (Hyvonen et al., 1995), Tiam1 and ArhGAP9 (Ceccarelli et al., 2007), and ASAP1 (Jian et al., 2015), where both canonical and atypical sites are simultaneously bound to short-chain PI(4,5)P<sub>2</sub>.

Notably, while the structures of PHA7<sub>APO</sub> and PHA7<sub>S</sub> are superimposable, with root-mean-square deviation (RMSD) of 0.49/0.52 Å (chains A-A/B-B) for CA atoms in the barrel core, they differ appreciably in the  $\beta$ 1- $\beta$ 2 loop where the RMSD jumps to 2.54/2.42 Å (chains A-A/B-B) (Figure S2B). In the apo structure, the  $\beta$ 1- $\beta$ 2 loop folds toward the barrel opening and adopts a  $\beta$ -turn conformation that is restrained by a network of hydrogen bonds involving the K173 and K183 amino groups, the S177 hydroxyl, and the D175 carboxylate oxygens (Figures 1A, S2C, and S2SD). The D175 side chain points into binding site I, at the center of a clasp-like structure formed by the K173 and K183 side chains. The temperature factors of the  $\beta$ 1- $\beta$ 2 loop are twice greater than for the rest of the protein, and the loop has a distinct conformation in each of the two molecules of the crystal structure, reflecting its flexibility (Figure S1C). In the sulfate-bound structure, on the other hand, the  $\beta$ 1- $\beta$ 2 loop folds away from the barrel opening (Figures 1B, S2C, and S2D). The D175 side chain is disengaged from the K173-K183 clasp: it points into the loop, forming hydrogen bonds with its main-chain atoms, and away from the sulfate anion bound in site I. The  $\beta$ 1- $\beta$ 2 temperature factors, while higher than those of the barrel proper, are lower than those observed in PHA7APO, and the loop has the same conformation in both molecules of the structure (Figure S1D), indicating that the bound sulfate stabilizes the  $\beta$ 1- $\beta$ 2 loop conformation.

The structures point to D175 and the  $\beta1$ - $\beta2$  loop as important mediators of the interaction of PHA7 with IP headgroups. A previous study (Carpten et al., 2007) identified a "sentry" Glu residue in the PH domain of AKT positioned to disfavor binding of a phosphate group at the 3-position of the inositol ring and define a preference for IP(4,5)P<sub>2</sub> over IP(3,4)P<sub>2</sub> and IP(3,4,5)P<sub>3</sub>. Changing this sentry Glu to Lys, an AKT mutation that occurs in many tumors, reverses the preference and increases the affinity for IPs by  $\sim$ 10-fold.



Table 1. ITC values of K<sub>D</sub> (μM) for the interactions of wild-type PHA7 or mutant PHA7-D175K with soluble IP headgroups or diC16phosphatidyl inositol (diC16-PI) incorporated in lipid nanodiscs

	IP(4,5)P <sub>2</sub> or PI(4,5)P <sub>2</sub>		IP(3,4,5)P <sub>3</sub> or PI(3,4,5)P <sub>3</sub>		IP(3,4)P <sub>2</sub> or PI(3,4)P <sub>2</sub>
	PHA7	PHA7-D175K	PHA7	PHA7-D175K	PHA7
Soluble IP	30.5 ± 0.6	10.7 ± 0.2	30.1 ± 2.3	3.5 ± 0.5	-
Nanodisc diC16-PI	3.0 ± 1.2	$0.5 \pm 0.1$	$6.2 \pm 0.2$	5.5 ± 0.1	$9.0 \pm 0.3$

To examine the role of D175 in PHA7, we generated the D175K mutant and characterized its structure and IP binding properties. ITC measurements show that PHA7-D175K has a 3-fold greater affinity for IP(4,5)P<sub>2</sub> ( $K_D = 10.7 \mu M$ ) and 9-fold greater affinity for  $IP(3,4,5)P_3$  (K<sub>D</sub> = 3.5  $\mu$ M) compared with wild type (Table 1). Notably, PHA7-D175K co-crystallized with soluble IP(3,4,5)P<sub>3</sub>. The structure refined to a resolution of 2.43 Å (Figure 1C and Table S1) with two copies of the protein per crystallographic asymmetric unit. Once again, no electron density was observed for the long β6-β7 loop, indicating that it remains mobile and disordered, without apparently contributing to IP binding.

The two molecules of PHA7-D175K within the crystallographic asymmetric unit coordinate two IP(3,4,5)P<sub>3</sub> moieties sandwiched between them: one at site I and the second associated more peripherally with yet another electropositive patch-denoted here as site III-formed by the side chains of K183, R185, K198, and R201 that protrude from  $\beta$ 2 and from the  $\beta$ 3- $\beta$ 4 loop (Figure S3A). The structure reflects at least four distinct modes of IP binding by PHA7. In molecule A of the asymmetric unit the phosphate group at the fifth position of the inositol ring occupies the same position as the sulfate anion in the structure of wild-type PHA7<sub>S</sub>, while in molecule B the binding geometry is flipped such that it is the phosphate group in the first position that coincides with the sulfate binding site (Figures S3B and S3C). Binding of the peripheral IP(3,4,5)P<sub>3</sub> at site III is similarly mirrored in each copy of PHA7-D175K, resulting in two possible binding geometries. Moreover, the involvement of K183 and R185 in both sites I and III reflects plasticity in the PHA7-IP interaction.

To further examine the interaction of wild-type PHA7 with IPs, we performed NMR experiments in solution. Addition of soluble IP(3,4,5)P<sub>3</sub> into <sup>15</sup>N-labeled PHA7 resulted in specific <sup>1</sup>H/<sup>15</sup>N chemical-shift perturbations that map to the PHA7 barrel opening (Figures 3A-3C). In line with the ITC data, NMR reflects a weak binding interaction with fast exchange binding dynamics (Williamson, 2013). No major structural reorganization of either the core or the  $\beta6-\beta7$  loop of PHA7 is observed, but signals from all three binding sites identified by crystallography are perturbed (Figures 3D and 3E), with the largest changes observed for the  $\beta$ 1- $\beta$ 2 and  $\beta$ 3- $\beta$ 4 loops and residues at the start of  $\beta$ 7, including key residues (Q174, D175, S177, K183, R185, Y260) identified in the structures of PHA7s and PHA7-D175K. We conclude that the interaction of PHA7 with soluble IP headgroups is structurally plastic, with three potential binding sites for inositol phosphate localized across the electropositive barrel opening, and low selectivity for a specific orientation of the IP(3,4,5)P<sub>3</sub> moiety.

#### Structural basis for binding membrane PIPs

The structural and ITC binding data show that PHA7 has modest affinity for freely soluble IP ligands but appreciably higher affinity for PIP-rich lipid bilayers, pointing to the importance of the PIP membrane environment. To explore the interaction with PIP membranes at the atomic level, we performed NMR experiments with <sup>15</sup>N-labeled PHA7 and PIP nanodiscs. Incubation of PHA7 with diC16-PC nanodiscs resulted in no detectable NMR spectral changes (Figure 4A and S4A). This is consistent with the liposome co-sedimentation results and confirms the inability of PHA7 to bind membranes devoid of PIP. Incubation with nanodiscs containing 10% molar diC16-PI(3,4,5)P<sub>3</sub> gave a dramatically different result: The NMR spectrum was effectively obliterated, except for peaks from sites in the termini and the flexible  $\beta6-\beta7$  loop (Figures 4B and S4B). We interpret such massive peak suppression to reflect immobilization of the relatively small 125-residue protein, caused by its association with the comparatively large nanodisc membrane. Moreover, since both PC and PIP nanodisc preparations have similar and homogeneous size distributions (~8 nm radius; Figure S4D), we attribute the peak suppression effect to a PIP-dependent association of the protein with the nanodisc membrane that is long-lived on the millisecond timescale of <sup>1</sup>H/<sup>15</sup>N correlation NMR experiments.

Increasing the temperature restored the NMR spectrum (Figures 4C and S4C), and while this is expected to enhance the binding exchange dynamics, it also allowed us to map specific chemical-shift perturbations that reflect the interaction of PHA7 with the PIP nanodisc membrane. The perturbations (Figure 4D) mirror the profile observed with free IP(3,4,5)P<sub>3</sub> (Figure 3D), but map to more extended regions of  $\beta 1$  and  $\beta 2$  and include sites in  $\beta$ 5- $\beta$ 6. The largest perturbations map to the  $\beta$ 1- $\beta$ 2 hairpin, the  $\beta$ 3- $\beta$ 4 loop, and the start of  $\beta$ 7, implicating binding sites I, II, and III in PIP-mediated membrane association, and indicating that PHA7 uses all three to dock onto the PIP membrane surface.

All-atom MD simulations provide molecular context for the NMR data. We performed ten independent, unrestrained, 1-μs MD simulations of PHA7 for each of three different lipid bilayer membranes similar to the experimental nanodiscs (Table S2). All ten simulations with either PI(4,5)P2 or PI(3,4,5)P3 resulted in rapid membrane surface association of PHA7, which remained membrane bound throughout the course of 1-μs simulation, while little evidence of binding to PC-only membranes was observed (Figures S5A-S5C). In all cases, PHA7 adopts a preferred orientation at the PIP membrane surface, with the  $\beta 3$ strand at an average angle of 35° from the membrane normal, the C-terminal helix exposed to bulk water, and sites I, II, and III docked on the membrane (Figures 4E, S5D, and S5E).

Notably, the interaction patterns from unrestrained MD simulations mirror the experimental NMR perturbation profile (Figures 5A and 5B). Protein sites with NMR signals that are sensitive to PIP nanodiscs also interact with the PIP membrane surface in the MD simulations. Viewed in a snapshot of MD simulation



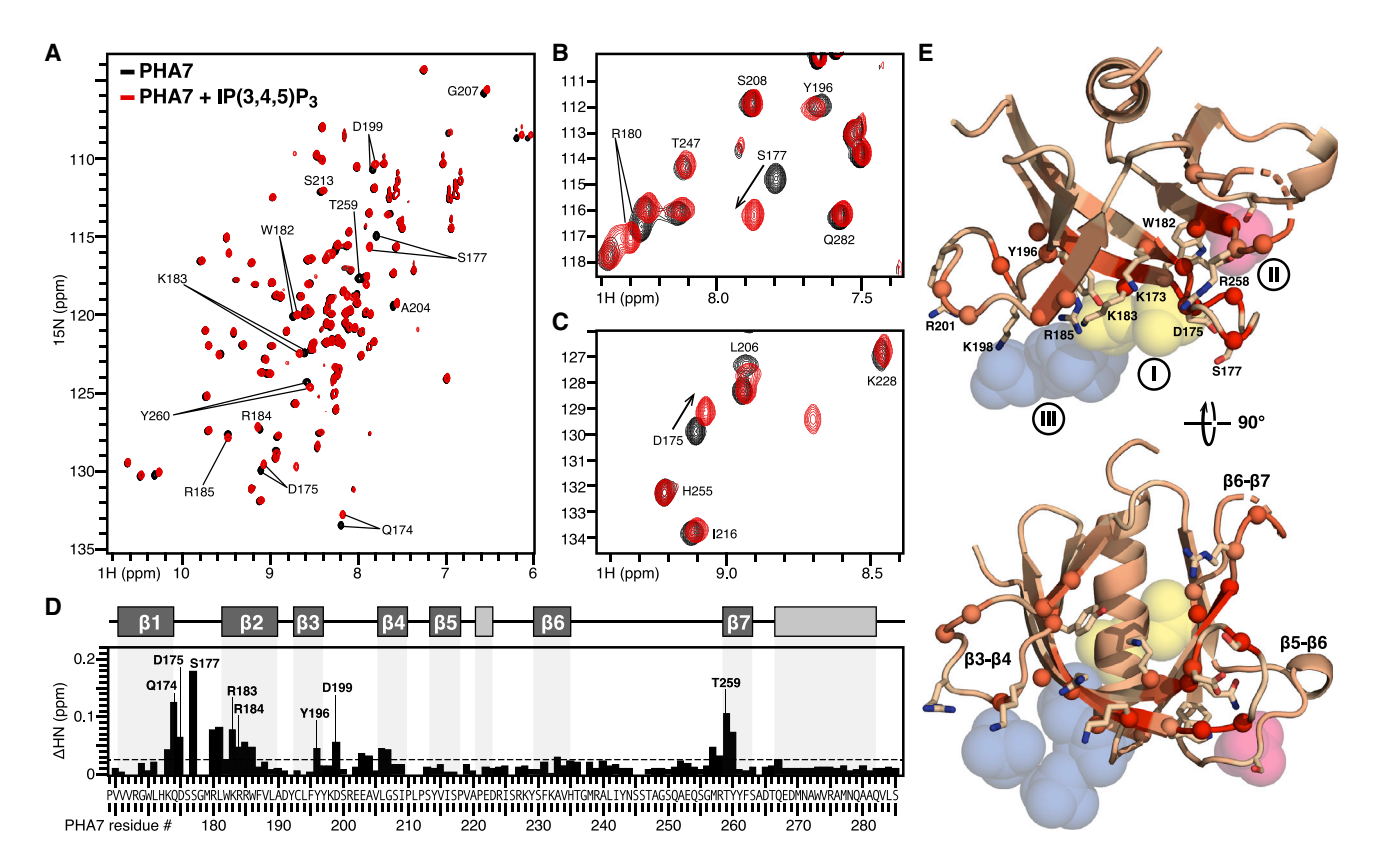


Figure 3. Interaction map of PHA7 with soluble IP(3,4,5)P<sub>3</sub>

(A–C) <sup>1</sup>H/<sup>15</sup>N heteronuclear single quantum coherence (HSQC) NMR spectra of <sup>15</sup>N labeled wild-type PHA7 domain acquired with (red) or without (black) 1.5 molar equivalents of soluble IP(3,4,5)P<sub>3</sub>. The spectra were acquired at 15°C. Selected regions of the spectra are expanded (B and C) to highlight specific perturbations.

(D) Profile of  ${}^{1}$ H ${}^{15}$ N chemical-shift perturbations induced by IP(3,4,5)P<sub>3</sub> across the sequence of PHA7. Bars represent the combined difference ( $\Delta$ HN) of amide  ${}^{1}$ H and  ${}^{15}$ N chemical shifts. The protein secondary structure is outlined at the top.

(E) Orthogonal views of the structure of PHA7<sub>APO</sub>. Colors reflect the magnitude of  $\Delta$ HN from 0 ppm (wheat) to the maximum value (red). Highly perturbed sites (>1 standard deviation of the values of  $\Delta$ HN) have CA atoms shown as spheres. Key side chains of three IP binding sites (I–III) are shown as sticks. The positions of sulfate or phosphate groups identified in the structures of PHA7<sub>S</sub> and PHA7-D175K are shown as spheres, superimposed on the structural model. They denote binding sites I (yellow), II, (pink), and III (blue).

with a PI(3,4,5)P $_3$  membrane (Figure 4E), the NMR perturbations are associated with membrane binding sites. These include conserved hydrophobic residues (L181, M179) in the  $\beta$ 1- $\beta$ 2 loop that insert deeply into the hydrophobic core of the membrane, thereby providing added stability to the interaction. The PH domain orientation at the membrane surface is remarkably similar to that observed from electron paramagnetic resonance-guided MD simulations of GPR1 with PIP membranes (Lai et al., 2013). In that study, hydrophobic interactions between GPR1 side chains and the membrane core were also observed, indicating that superficial membrane penetration helps stabilize a specific geometry of PH domain association with the membrane surface.

In line with this observation, the time-averaged root-mean-squared fluctuations (RMSFs), calculated for heavy atoms over the last 500 ns of 1- $\mu s$  MD trajectories, show that the  $\beta 1-\beta 2$  loop experiences a marked reduction in conformational flexibility upon binding PIP membranes (Figure 5C). By contrast, this effect is not observed for PC membranes. Moreover, while the long  $\beta 6-\beta 7$  loop remains highly flexible in both the soluble and membrane-associated states of PHA7, the length of its flexible region

is significantly reduced. At the molecular level, the loop fluctuations are dampened at its edges, where R239 and R258 engage with a PIP phosphate group and E253 helps stabilize the interaction.

Closer examination of the PHA7-PIP membrane assembly reveals multivalent interactions of the protein with PIPs. A total of seven PI(3,4,5)P $_3$  molecules establish close contacts (>4 Å) with the protein: Two PIP molecules associate with each of sites I and III, and three associate in the periphery of site II (Figures 5D and S5F). In this way, PHA7 recruits a cluster of PIP molecules to its periphery. The data demonstrate that PHA7 establishes multivalent interactions with membrane PIPs. These are primarily electrostatic, involving basic side chains and inositol ring phosphate groups, but also include hydrogen bonds from polar side chains and hydrophobic contacts between non-polar side chains and the lipid acyl chains. These results help explain the enhanced affinity of PHA7 for PIP membranes compared with freely soluble IPs.

Finally, we performed NMR experiments with short-chain diC8-PIP phospholipids into <sup>15</sup>N-labeled PHA7. The chemical-shift perturbations (Figure 6) mirror those observed with soluble



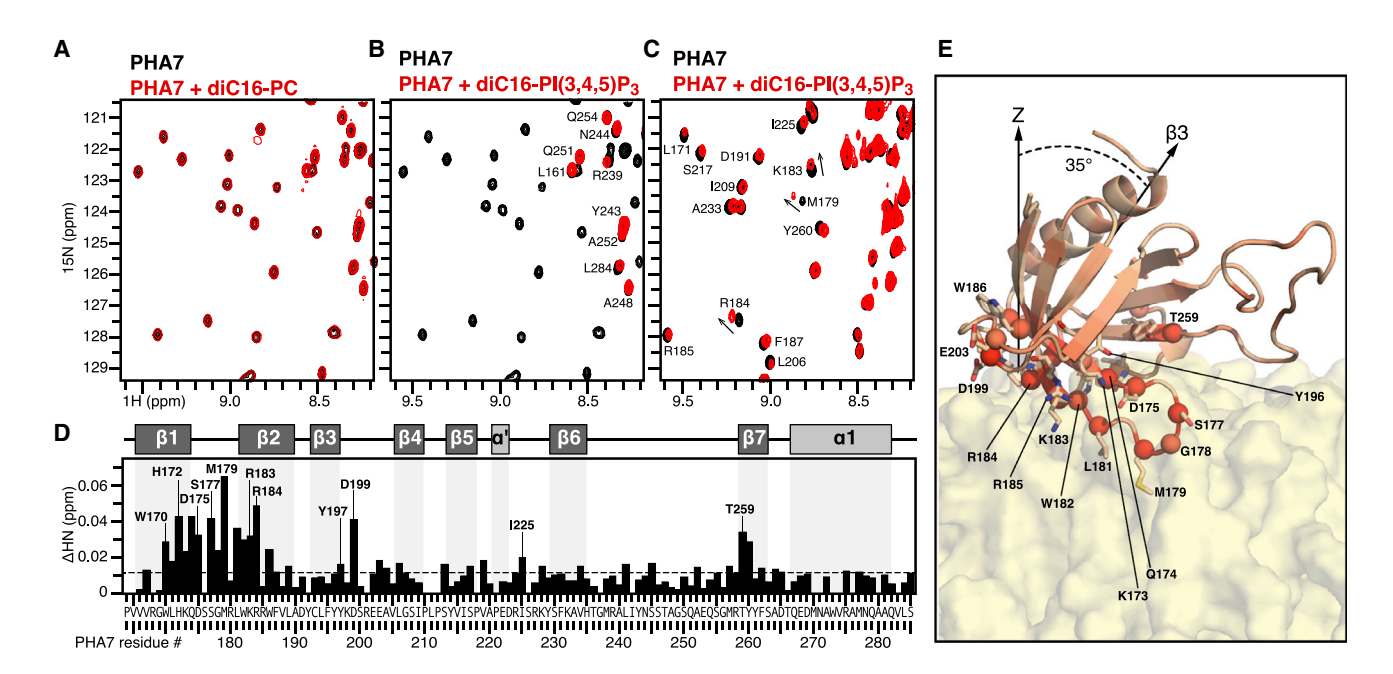


Figure 4. Interaction map of PLEKHA7 with diC16-PI(3,4,5)P<sub>3</sub> nanodiscs

(A-C) <sup>1</sup>H/<sup>15</sup>N HSQC NMR spectra of <sup>15</sup>N-labeled wild-type PHA7 obtained before (black) or after (red) incubation with 1.5 molar equivalents of lipid nanodiscs prepared with 100% diC16-PC (A) or 9/1 molar diC16-PC and diC16-PI(3,4,5)P3 (B, C). The spectra were acquired at 15°C (A and B) or 45°C (C). Peaks that do not change appreciably in the presence of diC16-PIP nanodiscs are labeled (B).

(D) Profile of <sup>1</sup>H/<sup>15</sup>N chemical-shift perturbations induced by the association of PHA7 with diC16-PI(3,4,5)P<sub>3</sub> nanodiscs, at 45°C, across the protein sequence. (E) Snapshot (taken at 890 ns) of an MD simulation of PHA7 with a diC16-PI(3,4,5)P<sub>3</sub>-rich lipid bilayer membrane. PHA7 colors reflect the magnitude of NMR chemical-shift perturbation from 0 ppm (wheat) to the maximum value (red). Highly perturbed sites (>1 standard deviation of the values of ΔHN) have CA atoms shown as spheres and side chains shown as sticks. The membrane is represented as a molecular surface. The β3 axis makes a 35° angle to the membrane normal (Z).

IP (Figure 3) and PIP nanodiscs (Figure 4), but also display notable differences: diC8-PIPs perturb additional hydrophobic sites (e.g., L188, C192, L193, I208, V273) deep inside the  $\beta$  barrel of the PH domain to helix  $\alpha 1$ , indicating that the acyl chains associate with hydrophobic patches in the barrel interior. Interestingly, association of the acyl chains with the β-barrel interior appears to be predicated upon binding of the PIP headgroup with PHA7, since the addition of non-phosphorylated diC8-PI induced no perturbations in the NMR spectrum of PHA7 (Figure 6A).

Caution must be exercised in interpreting the effects of micellar detergents such as diC8-PIPs, and we note that acyl chain penetration of the PH domain  $\beta$  barrel is not observed for PIP lipids embedded in the nanodisc membrane. Nonetheless, such interactions are not unprecedented, and may reflect an alternative function of the PH domain. For example, the serum retinol binding protein (Cowan et al., 1990) and fatty acid binding protein (Sacchettini et al., 1989) adopt a β-barrel structure that is very similar to that of PH domains, and each bind a retinol or acyl chain deep into their  $\beta$  barrel. Moreover, MD simulations of Grp1 with PIP membranes (Lumb et al., 2011) indicate that the Grp1 PH domain associates with membrane PIPs sufficiently tightly to pluck a single PIP phospholipid from the bilayer membrane assembly. In light of these studies, the finding that PIP lipid acyl chains associate with the PLEKHA7 PH β barrel is intriguing and suggestive of a functional role for the PH domain of PLEKHA7 that extends beyond membrane association, and may include lipid shuttling and regulation of PIP lipid mobility in the cell.

#### **Conclusions**

PLEKHA7 relies on the interactions of its PH domain with PIPs for proper localization to the plasma membrane surface and for its normal functions (Wythe et al., 2011). Using a multidisciplinary approach, we have defined the major elements of PIP recognition by the PLEKHA7 PH domain and have demonstrated the important role of the membrane scaffold in mediating its interaction with PIPs.

Although PH domains share a common fold and sequence homology, their PIP affinities and selectivities vary broadly. ITC shows that PLEKHA7 has modest affinity for free IP headgroups and no detectable selectivity for phosphorylation at specific inositol ring sites. By contrast, the binding affinity for PIP membranes is highly enhanced. Compared with freely soluble IP headgroups, the interaction with membrane PIPs is enthalpy driven and exhibits slight selectivity for PI(4,5)P2  $(>PI(3,4,5)P_3 > PI(3,4)P_2)$  relative to the other phosphorylation types. PI(4,5)P2 is the major PIP lipid present in the inner leaflet of the plasma membrane of mammalian cells. Its phosphorylation by PI 3-kinase (PI3K) produces PI(3,4,5)P3, a key second messenger in pathways related to cell survival and metabolism, while dephosphorylation of PI(3,4,5)P3 by phosphatases produces PI(3,4)P2 (Cantley, 2002). Low PIP selectivity is in line with the observations (Wythe et al., 2011) that PLEKHA7 membrane targeting is not linked to the PI3 kinase-dependent conversion of PI(4,5)P2 to PI(3,4,5)P3 in cells, and that its PH domain is promiscuous for phosphatidylinositol(4)monophosphate, PI(4,5)P<sub>2</sub>, and PI(3,4,5)P<sub>3</sub>, as well as other non-inositol



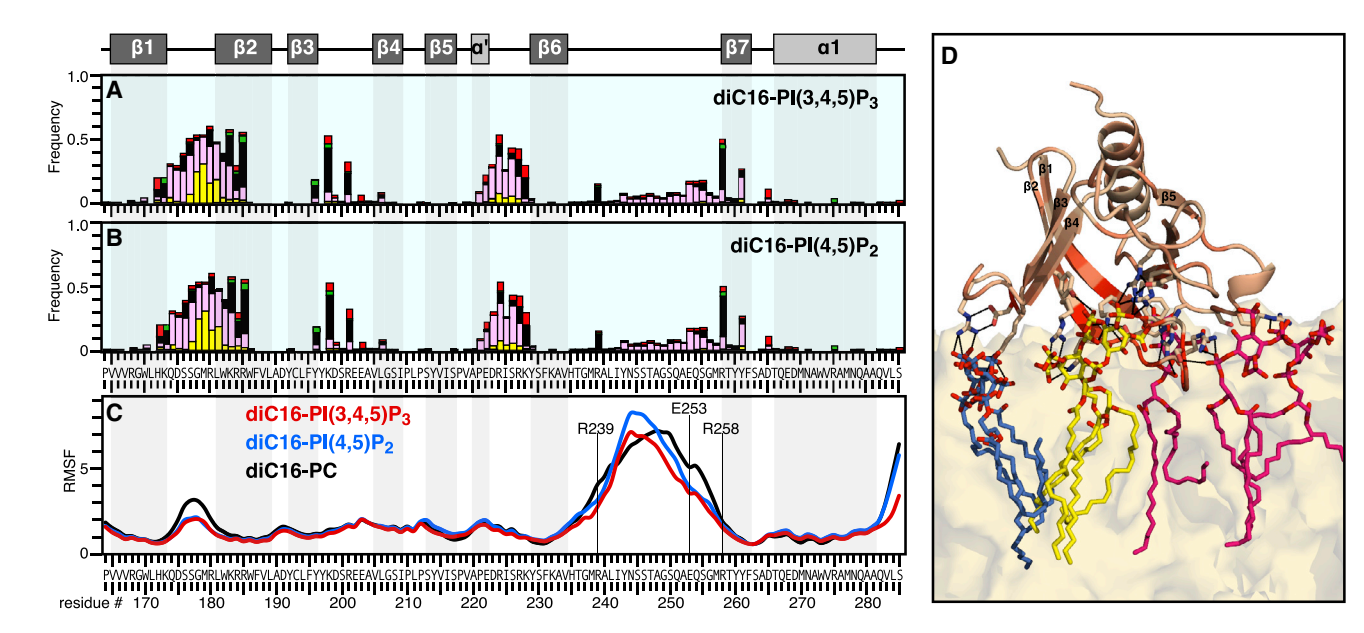


Figure 5. Structure and dynamics of the PLEKHA7 PH domain

(A and B) MD interaction profile of PHA7 with diC16-PI(3,4,5)P3 or diC16-PI(4,5)P2 membranes. The bars represent frequency of occurrence within 4 Å of water (light blue background), Na+ (red) or CI- (green) ions, phospholipid tails (yellow), PC headgroups (pink), or PIP headgroups (black). Each data point is the average of ten independent MD simulations over the last 500 ns of 1- $\mu s$  MD trajectories.

(C) MD time-averaged RMSF calculated for PHA7 heavy atoms over the last 500 ns of 1-μs MD trajectories for ten independent simulations in diC16-PI(3,4,5)P<sub>3</sub> (red), diC16-PI(4,5)P2 (blue), or diC16-PC (black) membranes.

(D) Snapshot (taken at 890 ns) of MD simulation of PHA7 with a diC16-PI(3,4,5)P3 membrane. PHA7 colors reflect the magnitude of NMR chemical-shift perturbation from 0 ppm (wheat) to the maximum value (red). Key side chains with close (<4 Å) contacts to PIP headgroups are shown as sticks. The membrane is represented as a molecular surface (yellow). Colors of bound PIP molecules (lines) represent their association with binding sites I (yellow), II (pink), or III (blue).

phospholipids with accessible phosphate groups, in lipid overlay assays.

Notwithstanding the relatively low selectivity of PLEKHA7 for specific inositol phosphates, the NMR data show that it does not bind short-chain diC8-Pl. We conclude, therefore, that phosphorylated inositol is required for binding PLEKHA7 and recruiting it to the membrane. While surface electrostatics from non-PIP acidic lipids, such as phosphatidylserine, has been shown to play a role in membrane recruitment of some PH domains (Lai et al., 2013), the data for PLEKHA7 indicate an affinity for phosphorylated inositol.

The crystal structures reveal three positively charged binding sites for the phosphate groups of the PIP headgroup moiety, and the NMR data show that all three sites engage with soluble IP headgroups, forming an extended binding surface at the open end of the PH domain  $\beta$  barrel. Notably, NMR studies with PIP nanodiscs show that the same binding sites, plus conserved hydrophobic residues in the β1-β2 loop, engage with membraneembedded PIPs leading to membrane surface association of the PH domain that is long-lived on the millisecond timescale. Moreover, the MD simulations show that PLEKHA7 interacts with the PIP membrane in two ways: by engaging the phosphate groups of multiple PIP molecules through electrostatic interactions with its three binding sites and by inserting hydrophobic side chains into the hydrophobic core of the lipid bilayer membrane. This multivalent binding interaction results in long-lived association of PH domain with the PIP membrane, on the microsecond timescale of the MD simulations.

The results further indicate that PLEKHA7 induces membrane PIP clustering. We note that our simplified nanodiscs and membrane systems have both restricted geometries and PIP concentrations that are ten times higher than cells-conditions that are likely to favor cluster formation. In cells, the reverse situation. where PLEKHA7 binds to preformed PIP clusters, is also possible. While the cellular levels of  $PI(4,5)P_2$  are low ( $\sim 1\%$  of total lipid), clustering is thought to increase its local concentration at specific membrane sites. A recent study (Wen et al., 2018) demonstrated that physiological levels of divalent and trivalent metal ions can induce cluster formation of very low PIP concentrations (<0.05 mol% of total lipids). The ability to form such cation-bridged PIP clusters at extremely low concentrations reveals an important property of this central lipid and provides evidence for the formation of distinct pools of PIP in cellular membranes, with fundamental consequences for biological function. As noted by Feigenson and colleagues (Wen et al., 2018), cation-induced PIP clustering would dampen the functions of proteins that bind free PIP lipids while enhancing the functions of proteins that bind clusters preferentially.

Clustering of PIP molecules around PH domains has also been observed in coarse-grained MD simulations, and has been proposed to contribute to the binding free energy (Yamamoto et al., 2020). Notably, two cooperative PIP binding sites have been observed experimentally in the PH domain of ASAP1, and this has been proposed to enable rapid switching between active and inactive states during cellular signaling (Jian et al., 2015). Association with multiple PI(4,5)P<sub>2</sub> molecules was recently shown

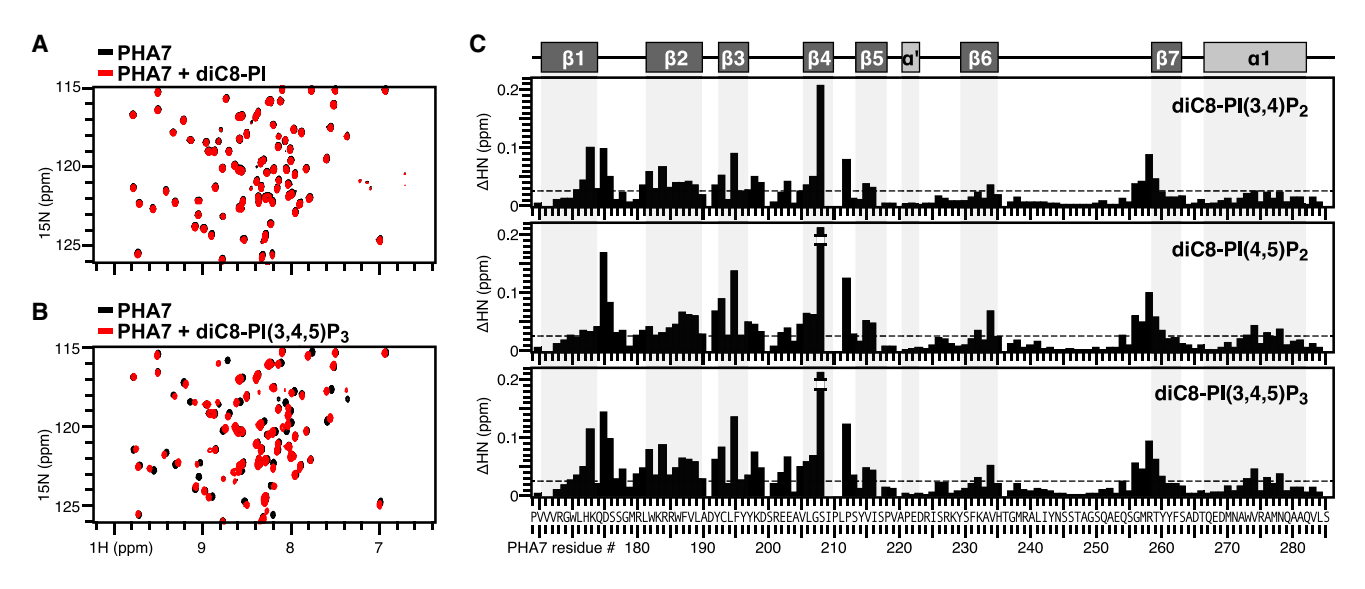


Figure 6. Interaction map of PHA7 with soluble short-chain diC8-PIPs

(A and B) Selected regions of the 1H/15N HSQC NMR spectra of 15N labeled wild-type PHA7 domain acquired with (red) or without (black) 1.5 molar equivalents of short-chain diC8-PI(3,4,5)P $_3$  or diC8-PI, at 15°C.

(C) Profiles of 1H/15N chemical-shift perturbations induced by diC8-PIPs across the sequence of PHA7. Bars represent the combined difference (ΔHN) of amide <sup>1</sup>H and <sup>15</sup>N chemical shifts. The protein secondary structure is outlined at the top.

to both trigger an allosteric conformational switch in the ASAP1 PH domain and maintain it in a well-defined orientation primed for functional protein-protein interactions, suggesting that PIP lipids have functionalities beyond simple membrane-targeting modules (Soubias et al., 2020). Notably, PIP-mediated membrane association has also been shown to regulate KRAS functionality (Cao et al., 2019), and this has potential implications for the role of PLEKHA7 in regulating the KRAS signaling nanocluster in colon cancer cells.

For PLEKHA7, we identified three binding sites and found that all three are engaged upon addition of either soluble IPs or PIP membranes, leading us to conclude that multivalent association is operative in both settings. Nevertheless, the membrane assembly is fundamentally important. The MD simulations indicate that PLEKHA7 establishes additional hydrophobic interactions with the membrane hydrocarbon core and adopts a preferred orientation at the membrane surface. Moreover, confinement of PIP molecules by the membrane scaffold reduces the degrees of freedom of the system to a single binding interface. We propose that these factors cooperate to lower the binding free energy and enhance the affinity of protein association with PIP membranes.

While most experimental studies have focused on the interactions of PH domains with soluble IP headgroups, our results provide atomic-level insights about the affinity of PLEKHA7 for full-length membrane-embedded PIPs. They highlight the central function of the membrane assembly and provide a roadmap for understanding how the functions of the PH domain integrate with the signaling, adhesion, and nanoclustering functions of fulllength PLEKHA7 in cells.

#### **STAR**\*METHODS

Detailed methods are provided in the online version of this paper and include the following:

- KEY RESOURCES TABLE
- RESOURCE AVAILABILITY
  - Lead contact
  - Materials availability
  - Data and code availability
- EXPERIMENTAL MODEL AND SUBJECT DETAILS
- METHOD DETAILS
  - Protein preparation
  - Nanodisc preparation
  - ITC experiments
  - O Liposome co-sedimentation assays
  - O Crystallization, X-Ray data acquisition and structure determination
  - NMR experiments
  - Molecular dynamics simulations
- QUANTIFICATION AND STATISTICAL ANALYSIS

#### SUPPLEMENTAL INFORMATION

Supplemental information can be found online at https://doi.org/10.1016/j.str. 2021.03.018.

#### **ACKNOWLEDGMENTS**

This work was supported by grants from the National Institutes of Health (GM118186, CA179087, CA160398, CA030199) and the National Science Foundation (MCB1810695).

#### **AUTHOR CONTRIBUTIONS**

Conceptualization and supervision, F.M.M., R.C.L., W.I., and G.P.; Investigation, A.E.A., Y.Y., J.Y., A.A.B., G.C., M.G.K., L.A.B., A.I., and C.D.; Writing original draft, F.M.M.; Writing - review & editing, F.M.M., A.E.A., Y.Y., and G.P.; Visualization, F.M.M. and A.E.A.; Funding acquisition and project administration, F.M.M., R.C.L., W.I., and G.P.





#### **DECLARATION OF INTERESTS**

G.P. is Director of PHusis Therapeutics. The authors declare no other competing interests.

Received: December 7, 2020 Revised: February 15, 2021 Accepted: March 25, 2021 Published: April 19, 2021

#### REFERENCES

Adams, P.D., Afonine, P.V., Bunkoczi, G., Chen, V.B., Davis, I.W., Echols, N., Headd, J.J., Hung, L.W., Kapral, G.J., Grosse-Kunstleve, R.W., et al. (2010). PHENIX: a comprehensive Python-based system for macromolecular structure solution. Acta Crystallogr. D. Biol. Crystallogr. 66, 213–221.

Awadalla, M.S., Thapa, S.S., Hewitt, A.W., Burdon, K.P., and Craig, J.E. (2013). Association of genetic variants with primary angle closure glaucoma in two different populations. PLoS One 8, e67903.

Baker, N.A., Sept, D., Joseph, S., Holst, M.J., and McCammon, J.A. (2001). Electrostatics of nanosystems: application to microtubules and the ribosome. Proc. Natl. Acad. Sci. U S A 98, 10037–10041.

Bax, A., and Grzesiek, S. (1993). Methodological advances in protein NMR. Acc. Chem. Res. 26, 131–138.

Bayburt, T.H., Grinkova, Y.V., and Sligar, S.G. (2002). Self-assembly of discoidal phospholipid bilayer nanoparticles with membrane scaffold proteins. Nano Lett. 2, 853–856.

Brooks, B.R., Brooks, C.L., 3rd, Mackerell, A.D., Jr., Nilsson, L., Petrella, R.J., Roux, B., Won, Y., Archontis, G., Bartels, C., Boresch, S., et al. (2009). CHARMM: the biomolecular simulation program. J. Comput. Chem. *30*, 1545–1614.

Cantley, L.C. (2002). The phosphoinositide 3-kinase pathway. Science 296, 1655–1657.

Cao, S., Chung, S., Kim, S., Li, Z., Manor, D., and Buck, M. (2019). K-Ras G-domain binding with signaling lipid phosphatidylinositol (4,5)-phosphate (PIP2): membrane association, protein orientation, and function. J. Biol. Chem. 294, 7068–7084.

Carpten, J.D., Faber, A.L., Horn, C., Donoho, G.P., Briggs, S.L., Robbins, C.M., Hostetter, G., Boguslawski, S., Moses, T.Y., Savage, S., et al. (2007). A transforming mutation in the pleckstrin homology domain of AKT1 in cancer. Nature 448. 439–444.

Castellana, B., Escuin, D., Perez-Olabarria, M., Vazquez, T., Munoz, J., Peiro, G., Barnadas, A., and Lerma, E. (2012). Genetic up-regulation and overexpression of PLEKHA7 differentiates invasive lobular carcinomas from invasive ductal carcinomas. Hum. Pathol. *43*, 1902–1909.

Cavanagh, J., Fairbrother, W.J., Palmer, A.G., and Skelton, N.J. (1996). Protein NMR Spectroscopy: Principles and Practice (Academic Press).

Ceccarelli, D.F., Blasutig, I.M., Goudreault, M., Li, Z., Ruston, J., Pawson, T., and Sicheri, F. (2007). Non-canonical interaction of phosphoinositides with pleckstrin homology domains of Tiam1 and ArhGAP9. J. Biol. Chem. 282, 13864–13874.

Chen, V.B., Arendall, W.B., 3rd, Headd, J.J., Keedy, D.A., Immormino, R.M., Kapral, G.J., Murray, L.W., Richardson, J.S., and Richardson, D.C. (2010). MolProbity: all-atom structure validation for macromolecular crystallography. Acta Crystallogr. D. Biol. Crystallogr. 66, 12–21.

Clore, G.M., and Gronenborn, A.M. (1998). NMR structure determination of proteins and protein complexes larger than 20 kDa. Curr. Opin. Chem. Biol. 2, 564–570.

Cornilescu, G., Delaglio, F., and Bax, A. (1999). Protein backbone angle restraints from searching a database for chemical shift and sequence homology. J. Biomol. NMR *13*, 289–302.

Cowan, S.W., Newcomer, M.E., and Jones, T.A. (1990). Crystallographic refinement of human serum retinol binding protein at 2A resolution. Proteins 8 44–61

Cronin, T.C., DiNitto, J.P., Czech, M.P., and Lambright, D.G. (2004). Structural determinants of phosphoinositide selectivity in splice variants of Grp1 family PH domains. EMBO J. 23, 3711–3720.

Delaglio, F., Grzesiek, S., Vuister, G.W., Zhu, G., Pfeifer, J., and Bax, A. (1995). NMRPipe: a multidimensional spectral processing system based on UNIX pipes. J. Biomol. NMR 6, 277–293.

DeLano, W.L. (2002). PyMOL: an open-source molecular graphics tool. CCP4 Newslett. Protein Crystallogr. 1, 82–92.

Ding, Y., Fujimoto, L.M., Yao, Y., Plano, G.V., and Marassi, F.M. (2015). Influence of the lipid membrane environment on structure and activity of the outer membrane protein Ail from Yersinia pestis. Biochim. Biophys. Acta 1848, 712–720.

DiNitto, J.P., and Lambright, D.G. (2006). Membrane and juxtamembrane targeting by PH and PTB domains. Biochim. Biophys. Acta 1761, 850–867.

Eastman, P., Friedrichs, M.S., Chodera, J.D., Radmer, R.J., Bruns, C.M., Ku, J.P., Beauchamp, K.A., Lane, T.J., Wang, L.P., Shukla, D., et al. (2013). OpenMM 4: a reusable, extensible, hardware independent library for high performance molecular simulation. J. Chem. Theor. Comput. 9, 461–469.

Emsley, P., Lohkamp, B., Scott, W.G., and Cowtan, K. (2010). Features and development of Coot. Acta Crystallogr. D. Biol. Crystallogr. 66, 486–501.

Ferentz, A.E., and Wagner, G. (2000). NMR spectroscopy: a multifaceted approach to macromolecular structure. Q. Rev. Biophys. 33, 29–65.

Ferguson, K.M., Kavran, J.M., Sankaran, V.G., Fournier, E., Isakoff, S.J., Skolnik, E.Y., and Lemmon, M.A. (2000). Structural basis for discrimination of 3-phosphoinositides by pleckstrin homology domains. Mol. Cell *6*, 373–384.

Fesik, S.W., and Zuiderweg, E.R. (1990). Heteronuclear three-dimensional NMR spectroscopy of isotopically labelled biological macromolecules. Q. Rev. Biophys. *23*, 97–131.

Goddard, T.D., and Kneller, D.G. (2004). SPARKY 3 (University of California). Grzesiek, S., and Bax, A. (1992). Improved 3D triple-resonance NMR techniques applied to a 31 kDa protein. J. Magn. Reson. 96, 432–440.

Hagn, F., Etzkorn, M., Raschle, T., and Wagner, G. (2013). Optimized phospholipid bilayer nanodiscs facilitate high-resolution structure determination of membrane proteins. J. Am. Chem. Soc. *135*, 1919–1925.

Humphrey, W., Dalke, A., and Schulten, K. (1996). VMD: visual molecular dynamics. J. Mol. Graph. 14, 27–38.

Hyvonen, M., Macias, M.J., Nilges, M., Oschkinat, H., Saraste, M., and Wilmanns, M. (1995). Structure of the binding site for inositol phosphates in a PH domain. EMBO J. *14*, 4676–4685.

Indarte, M., Puentes, R., Maruggi, M., Ihle, N.T., Grandjean, G., Scott, M., Ahmed, Z., Meuillet, E.J., Zang, S., Lemos, R., Jr., et al. (2019). An inhibitor of the pleckstrin homology domain of CNK1 selectively blocks the growth of mutant KRAS cells and tumors. Cancer Res. 79, 3100–3111.

Jencks, W.P. (1981). On the attribution and additivity of binding energies. Proc. Natl. Acad. Sci. U S A 78, 4046–4050.

Jeung, H.-C., Kiriakova, G., Kirkpatrick, L., Indarte, M., and Powis, G. (2011). Abstract A199: the plekstrin-homology-domain-containing protein PLEKHA7 is a novel target for selectively inhibiting mutant KRAS colon cancer cell proliferation. Mol. Cancer Ther. *10*, A199.

Jian, X., Tang, W.K., Zhai, P., Roy, N.S., Luo, R., Gruschus, J.M., Yohe, M.E., Chen, P.W., Li, Y., Byrd, R.A., et al. (2015). Molecular basis for cooperative binding of anionic phospholipids to the PH domain of the arf GAP ASAP1. Structure *23*, 1977–1988.

Jo, S., Kim, T., Iyer, V.G., and Im, W. (2008). CHARMM-GUI: a web-based graphical user interface for CHARMM. J. Comput. Chem. 29, 1859–1865.

Jo, S., Lim, J.B., Klauda, J.B., and Im, W. (2009). CHARMM-GUI Membrane Builder for mixed bilayers and its application to yeast membranes. Biophys. J. 97. 50–58.

Johnson, B.A., and Blevins, R.A. (1994). NMR View: a computer program for the visualization and analysis of NMR data. J. Biomol. NMR 4, 603–614.

Jorgensen, W.L., Chandrasekhar, J., Madura, J.D., Impey, R.W., and Klein, M.L. (1983). Comparison of simple potential functions for simulating liquid water. J. Chem. Phys. *79*, 926–935.

#### **Article**



Kay, L.E. (2001). Nuclear magnetic resonance methods for high molecular weight proteins: a study involving a complex of maltose binding protein and beta-cyclodextrin. Methods Enzymol. 339, 174-203.

Klauda, J.B., Venable, R.M., Freites, J.A., O'Connor, J.W., Tobias, D.J., Mondragon-Ramirez, C., Vorobyov, I., MacKerell, A.D., Jr., and Pastor, R.W. (2010). Update of the CHARMM all-atom additive force field for lipids: validation on six lipid types. J. Phys. Chem. B 114, 7830-7843.

Ko, J., Lee, D., Park, H., Coutsias, E.A., Lee, J., and Seok, C. (2011). The FALC-Loop web server for protein loop modeling. Nucleic Acids Res. 39, W210-W214.

Kourtidis, A., Ngok, S.P., Pulimeno, P., Feathers, R.W., Carpio, L.R., Baker, T.R., Carr, J.M., Yan, I.K., Borges, S., Perez, E.A., et al. (2015). Distinct E-cadherin-based complexes regulate cell behaviour through miRNA processing or Src and p120 catenin activity. Nat. Cell Biol. 17, 1145-1157.

Lai, C.L., Srivastava, A., Pilling, C., Chase, A.R., Falke, J.J., and Voth, G.A. (2013). Molecular mechanism of membrane binding of the GRP1 PH domain. J. Mol. Biol. 425, 3073-3090.

Lee, J., Patel, D.S., Stahle, J., Park, S.J., Kern, N.R., Kim, S., Lee, J., Cheng, X., Valvano, M.A., Holst, O., et al. (2019). CHARMM-GUI membrane builder for complex biological membrane simulations with glycolipids and lipoglycans. J. Chem. Theor. Comput. 15, 775-786.

Lemmon, M.A. (2007). Pleckstrin homology (PH) domains and phosphoinositides. Biochem. Soc. Symp. 81-93.

Lenoir, M., Coskun, U., Grzybek, M., Cao, X., Buschhorn, S.B., James, J., Simons, K., and Overduin, M. (2010). Structural basis of wedging the Golgi membrane by FAPP pleckstrin homology domains. EMBO Rep. 11, 279–284.

Levy, D., Ehret, G.B., Rice, K., Verwoert, G.C., Launer, L.J., Dehghan, A., Glazer, N.L., Morrison, A.C., Johnson, A.D., Aspelund, T., et al. (2009). Genome-wide association study of blood pressure and hypertension. Nat. Genet. 41, 677-687.

Lietzke, S.E., Bose, S., Cronin, T., Klarlund, J., Chawla, A., Czech, M.P., and Lambright, D.G. (2000). Structural basis of 3-phosphoinositide recognition by pleckstrin homology domains. Mol. Cell 6, 385-394.

Lumb, C.N., He, J., Xue, Y., Stansfeld, P.J., Stahelin, R.V., Kutateladze, T.G., and Sansom, M.S. (2011). Biophysical and computational studies of membrane penetration by the GRP1 pleckstrin homology domain. Structure 19,

Macias, M.J., Musacchio, A., Ponstingl, H., Nilges, M., Saraste, M., and Oschkinat, H. (1994). Structure of the pleckstrin homology domain from beta-spectrin. Nature 369, 675-677.

McCoy, A.J., Grosse-Kunstleve, R.W., Adams, P.D., Winn, M.D., Storoni, L.C., and Read, R.J. (2007). Phaser crystallographic software. J. Appl. Crystallogr.

Meng, W., Mushika, Y., Ichii, T., and Takeichi, M. (2008). Anchorage of microtubule minus ends to adherens junctions regulates epithelial cell-cell contacts. Cell 135, 948-959.

Meuillet, E.J., Mahadevan, D., Vankayalapati, H., Berggren, M., Williams, R., Coon, A., Kozikowski, A.P., and Powis, G. (2003). Specific inhibition of the Akt1 pleckstrin homology domain by D-3-deoxy-phosphatidyl-myo-inositol analogues. Mol. Cancer Ther. 2, 389-399.

Meuillet, E.J., Zuohe, S., Lemos, R., Ihle, N., Kingston, J., Watkins, R., Moses, S.A., Zhang, S., Du-Cuny, L., Herbst, R., et al. (2010). Molecular pharmacology and antitumor activity of PHT-427, a novel Akt/phosphatidylinositide-dependent protein kinase 1 pleckstrin homology domain inhibitor. Mol. Cancer Ther. 9, 706-717.

Moravcevic, K., Oxley, C.L., and Lemmon, M.A. (2012). Conditional peripheral membrane proteins: facing up to limited specificity. Structure 20, 15-27.

Murshudov, G.N., Skubák, P., Lebedev, A.A., Pannu, N.S., Steiner, R.A., Nicholls, R.A., Winn, M.D., Long, F., and Vagin, A.A. (2011). REFMAC5 for the refinement of macromolecular crystal structures. Acta Crystallographica. Section D, Biol. Crystallogr. 67, 355-367.

Nair-Menon, J., Daulagala, A.C., Connor, D.M., Rutledge, L., Penix, T., Bridges, M.C., Wellslager, B., Spyropoulos, D.D., Timmers, C.D., Broome, A.M., et al. (2020). Predominant distribution of the RNAi machinery at apical adherens junctions in colonic epithelia is disrupted in cancer. Int. J. Mol. Sci.

Ni, T., Kalli, A.C., Naughton, F.B., Yates, L.A., Naneh, O., Kozorog, M., Anderluh, G., Sansom, M.S., and Gilbert, R.J. (2017). Structure and lipid-binding properties of the kindlin-3 pleckstrin homology domain. Biochem. J. 474,

Paschoud, S., Jond, L., Guerrera, D., and Citi, S. (2014). PLEKHA7 modulates epithelial tight junction barrier function. Tissue Barriers 2, e28755.

Pulimeno, P., Bauer, C., Stutz, J., and Citi, S. (2010). PLEKHA7 is an adherens junction protein with a tissue distribution and subcellular localization distinct from ZO-1 and E-cadherin, PLoS One 5, e12207.

Rouaud, F., Sluysmans, S., Flinois, A., Shah, J., Vasileva, E., and Citi, S. (2020). Scaffolding proteins of vertebrate apical junctions: structure, functions and biophysics. Biochim. Biophys. Acta Biomembr. 1862, 183399.

Sacchettini, J.C., Gordon, J.I., and Banaszak, L.J. (1989). Crystal structure of rat intestinal fatty-acid-binding protein. Refinement and analysis of the Escherichia coli-derived protein with bound palmitate. J. Mol. Biol. 208,

Shen, Y., Delaglio, F., Cornilescu, G., and Bax, A. (2009). TALOS+: a hybrid method for predicting protein backbone torsion angles from NMR chemical shifts. J. Biomol. NMR 44, 213-223.

Soubias, O., Pant, S., Heinrich, F., Zhang, Y., Roy, N.S., Li, J., Jian, X., Yohe, M.E., Randazzo, P.A., Losche, M., et al. (2020). Membrane surface recognition by the ASAP1 PH domain and consequences for interactions with the small GTPase Arf1, Sci. Adv. 6, eabd1882.

Thomas, C.C., Dowler, S., Deak, M., Alessi, D.R., and van Aalten, D.M. (2001). Crystal structure of the phosphatidylinositol 3,4-bisphosphate-binding pleckstrin homology (PH) domain of tandem PH-domain-containing protein 1 (TAPP1): molecular basis of lipid specificity. Biochem. J. 358, 287-294.

Tille, J.C., Ho, L., Shah, J., Seyde, O., McKee, T.A., and Citi, S. (2015). The expression of the zonula adhaerens protein PLEKHA7 is strongly decreased in high grade ductal and lobular breast carcinomas. PLoS One 10, e0135442.

Wen, Y., Vogt, V.M., and Feigenson, G.W. (2018). Multivalent cation-bridged PI(4,5)P2 clusters form at very low concentrations. Biophys. J. 114, 2630-2639.

Williamson, M.P. (2013). Using chemical shift perturbation to characterise ligand binding. Prog. Nucl. Magn. Reson. Spectrosc. 73, 1-16.

Winn, M.D., Ballard, C.C., Cowtan, K.D., Dodson, E.J., Emsley, P., Evans, P.R., Keegan, R.M., Krissinel, E.B., Leslie, A.G., McCoy, A., et al. (2011). Overview of the CCP4 suite and current developments. Acta Crystallogr. D. Biol. Crystallogr. 67, 235-242.

Wittekind, M., and Mueller, L. (1993). HNCACB, a high-sensitivity 3D NMR experiment to correlate amide-proton and nitrogen resonances with the alphaand beta-carbon resonances in proteins. J. Magn. Reson. B 101, 201-205.

Wythe, J.D., Jurynec, M.J., Urness, L.D., Jones, C.A., Sabeh, M.K., Werdich, A.A., Sato, M., Yost, H.J., Grunwald, D.J., Macrae, C.A., et al. (2011). Hadp1, a newly identified pleckstrin homology domain protein, is required for cardiac contractility in zebrafish. Dis. Model. Mech. 4, 607-621.

Yamamoto, E., Domanski, J., Naughton, F.B., Best, R.B., Kalli, A.C., Stansfeld, P.J., and Sansom, M.S.P. (2020). Multiple lipid binding sites determine the affinity of PH domains for phosphoinositide-containing membranes. Sci. Adv. 6, eaav5736.

Yoon, H.S., Hajduk, P.J., Petros, A.M., Olejniczak, E.T., Meadows, R.P., and Fesik, S.W. (1994). Solution structure of a pleckstrin-homology domain. Nature 369, 672-675.





#### **STAR**\***METHODS**

#### **KEY RESOURCES TABLE**

REAGENT or RESOURCE	SOURCE	IDENTIFIER
Bacterial and virus strains		
E. coli BL21(DE3) cells	Invitrogen	Cat: C600003
Chemicals, peptides, and recombinant proteins		
( <sup>15</sup> NH <sub>4</sub> ) <sub>2</sub> SO <sub>4</sub>	Cambridge Isotope Laboratories	NLM-713
<sup>13</sup> C-glucose	Cambridge Isotope Laboratories	CLM-1396
diC16-PC	Avanti Polar Lipids	850355
diC16-PI(4,5)P <sub>2</sub>	Echelon	P-4516
diC16-PI(3,4)P <sub>2</sub>	Echelon	P-3416
diC16-PI(3,4,5)P <sub>3</sub>	Echelon	P-3916
Deposited data		
Structure of PLEKHA7 PH domain (PHA7 <sub>APO</sub> )	This paper	PDB: 7kk7
crystal structure of PLEKHA7 PH domain biding SO4 (PHA7 <sub>S</sub> )	This paper	PDB: 7kjo
crystal structure of PLEKHA7 PH domain biding inositol-tetraphosphate (PHA7-D175K)	This paper	PDB: 7kjz
NMR chemical shifts of PLEKHA7 PH domain	This paper	BMRB: 50512
Structure of PLEKHA1 PH domain (PHA1)	(Thomas et al., 2001)	PDB: 1eaz
Structure of PLEKHA3 PH domain (PHA3)	(Lenoir et al., 2010)	PDB: 2kcj
Structure of PLEKHA4 PH domain (PHA4)	unpublished data.	PDB: 1upq
Structure of PLEKHA5 PH domain (PHA5)	unpublished data.	PDB: 2dkp
Structure of PLEKHA6 PH domain (PHA6)	unpublished data.	PDB: 2yry
Structure of ANLN PH domain	unpublished data.	PDB: 2y7b
Structure of GRP1 PH domain	(Lietzke et al., 2000)	PDB: 1fgy
Structure of ARNO PH domain	(Cronin et al., 2004)	PDB: 1u27
Structure of DAPP1 PH domain	(Ferguson et al., 2000)	PDB: 1fao
Software and algorithms		
NMRPipe	(Delaglio et al., 1995)	https://spin.niddk.nih.gov/bax/software/ NMRPipe/NMRPipe.html
Sparky	(Goddard and Kneller, 2004)	https://www.cgl.ucsf.edu/home/sparky/
NMRView	(Johnson and Blevins, 1994)	http://www.onemoonscientific.com/
TopSpin	Bruker Biospin	https://www.bruker.com/products/mr/nmr/software/topspin.html
PyMol	Schroedinger (DeLano, 2002)	https://pymol.org/2/
PHENIX	(Adams et al., 2010)	http://www.phenix-online.org/
CCP4	(Winn et al., 2011)	http://www.ccp4.ac.uk/
COOT	(Emsley et al., 2010)	https://www2.mrc-lmb.cam.ac.uk/ personal/pemsley/coot/
Molprobity	(Chen et al., 2010)	http://molprobity.biochem.duke.edu/
CHARMM36(m)	(Brooks et al., 2009; Klauda et al., 2010)	https://www.charmm.org/
CHARMM-GUI	(Jo et al., 2008, 2009; Lee et al., 2019)	http://www.charmm-gui.org/

#### **RESOURCE AVAILABILITY**

#### **Lead contact**

Further information and requests for resources and reagents should be directed to and will be fulfilled by the lead contact, Francesca M. Marassi (fmarassi@sbp.edu).

#### Article



#### **Materials availability**

Plasmids generated in this study are available upon request.

#### Data and code availability

The structural atomic coordinates generated in this study are available at the Protein DataBank (accession codes PDB: 7kk7, 7kjo and 7kjz). The assigned NMR chemical shifts are available at the BMRB databank (accession code BMRB: 50512).

#### **EXPERIMENTAL MODEL AND SUBJECT DETAILS**

E. coli BL21 cells were used for protein expression and purification. For crystallography and ITC the bacterial cells were grown at 37°C, in LB media. For NMR studies, the bacteria were grown in M9 minimal media containing (15NH<sub>4</sub>)<sub>2</sub>SO<sub>4</sub> and/or 13C-glucose (Cambridge Isotope Laboratories), to obtain isotopically labeled protein.

#### **METHOD DETAILS**

#### Protein preparation

The sequences (Figure S1B) of human PLEKHA7 were cloned into the BamHI and XhoI restriction sites of the pGEX-6P-1 plasmid, and expressed in E. coli BL21 cells. For crystallography and ITC the bacterial cells were grown at 37°C, in LB media. For NMR studies, the bacteria were grown in M9 minimal media containing (15NH<sub>4</sub>)<sub>2</sub>SO<sub>4</sub> and/or 13C-glucose (Cambridge Isotope Laboratories), to obtain isotopically labeled protein. Protein expression was induced by adding 1 mM isopropyl-1-thio-β-D-galactopyranoside to the culture when the cell optical density at 600 nm (OD<sub>600</sub>) reached 0.6. After growing the cells for an additional 15 hr at 18°C, they were harvested by centrifugation (6,000 x g, 4°C, 15 min) and stored at -80°C overnight. Cells harvested from 2 L of culture were suspended in 35 mL of buffer A (25 mM Na/K phosphate, pH 7.4, 200 mM NaCl, 2 mM DTT, 1 mM EDTA), supplemented with protease inhibitors (cOmplete Mini EDTA-free cocktail; Roche), and lysed using a French Press.

The soluble fraction was isolated as the supernatant from centrifugation after cell lysis, and loaded on Glutathione Sepharose beads (GE Healthcare). The beads were washed with buffer B (25 mM Na/K phosphate, pH 7.4, 500 mM NaCl, 2 mM DTT, 1 mM EDTA), and then incubated overnight, at 40°C, with HRV 3C Protease (Genscript; 1.5 units per 1 mg of fusion protein) in buffer C (20 mM HEPES pH 7.4, 100 mM NaCl, 1 mM DTT, 1 mM EDTA). The cleaved protein was eluted with buffer II and further purified by cation exchange chromatography (HiTrap SP column, 5 mL, GE Healthcare) with a linear gradient of NaCl in buffer D (20 mM Tris-Cl, pH 8, 1 mM DTT, 1 mM EDTA).

Purified protein was concentrated to 10 mg/mL and stored frozen at -80°C. Prior to use, the protein was thawed, transferred to appropriate buffer by size exclusion chromatography (Superdex 75 10/300, GE Healthcare), then concentrated by centrifugal ultrafiltration and kept at 4°C. Samples for NMR studies were transferred to NMR buffer (20 mM MES pH 6.0, 100 mM NaCl, 1 mM TCEP, 1 mM EDTA). For studies of PLEKHA7 with nanodiscs, the purified PH domain was added directly to preformed nanodiscs prepared in NMR buffer.

#### **Nanodisc preparation**

Nanodiscs were prepared as described previously (Ding et al., 2015). Briefly, the phospholipids were dissolved in 1 mL of nanodisc buffer (20 mM Tris-CI, pH 7.5, 100 mM NaCI, 1 mM EDTA) supplemented with Na-cholate to obtain a final 2:1 molar ratio of cholate per lipid. MSP1D1Δh5 was produced in E. coli, as described (Hagn et al., 2013), then dissolved in 700 μL of nanodisc buffer, and combined with the lipid solution. After incubation at room temperature for 1 hr, 2 g of Biobeads SM-2 (Biorad), prewashed in nanodisc buffer, were added, and the mixture was further incubated at room temperature, with gentle mixing, for 12 hr. The Biobeads were removed by centrifugation (1,000 x g, 4°C, 5 min) and the resulting nanodiscs were washed twice with one sample volume of nanodisc buffer. The nanodisc solution was concentrated using a 10 kD cutoff Vivaspin concentrator (Viva Products) and replaced with NMR buffer to obtain 500 μL of 0.2 mM nanodiscs. The nanodisc concentration was estimated by measuring absorbance at 280 nm  $(A_{280})$  of MSP1D1 $\Delta$ h5, of which there are two copies per nanodisc. The distribution of PIP molecules among nanodiscs is assumed to be homogeneous, but this may not be the case. Nanodiscs were prepared with 100% diC16-PC, or 9/1 molar mixtures of diC16-PC with diC16-PI(3,4,5)P<sub>3</sub>, diC16-PI(4,5)P<sub>2</sub>, or diC16-PI(3,4)P<sub>2</sub>. Analytical size exclusion chromatography (Superdex 75 10/300 GL column, GE Healthcare) was performed in NMR buffer to assess nanodisc size homogeneity.

#### **ITC** experiments

ITC experiments were performed at 23°C, with all components in ITC buffer (15 mM Tris pH 7.6, 70 mM NaCl, 0.5 mM TCEP), using an iTC200 instrument (MicroCal). Titrations with soluble IP headgroups were performed with 50 μM PHA7 in the ITC cell and 0.5 mM soluble IP molecules in the injection syringe. Titrations with PIP nanodiscs were performed with 15 μM nanodiscs in the ITC cell and 0.5 mM PHA7 in the injection syringe. The protein concentrations were estimated by measuring A<sub>280</sub>. Nanodisc concentrations reflect the A<sub>280</sub> measurement of MSP1D1Δh5. Integrated heat data were processed and analyzed with ORIGIN software (Microcal version 7.0552). The data were fit to a single-site binding model to extract the values of the dissociation constant for each titration.





#### Liposome co-sedimentation assays

Dry lipids, either 100% diC16-PC, or a 9/1 molar mixture of diC16-PC and diC16-PI(4,5)P2, were suspended in 2 mL of buffer (20 mM MES pH 6.0, 100 mM NaCl, 2 mM DTT, 1 mM EDTA) at a concentration of 3 mg/mL, then sonicated in a bath sonicator until the suspension became translucent, marking the formation of small unilamellar vesicles. A 200 uL solution of vesicles was mixed with a 20 uM solution of PLEKHA7 and incubated at room temperature for 2 hr. Liposomes were then harvested by centrifugation in a BECKMAN Airfuge (A-100/30 rotor, 91,000 rpm) for 20 hr. The supernatant and sediment fractions were separated and analyzed by SDS-PAGE.

#### Crystallization, X-Ray data acquisition and structure determination

All PHA7 crystals were obtained using the sitting drop method. For ligand-free PHA7<sub>APO</sub>, protein solution (13 mg/mL in 180 mM NaCl, 20 mM Tris pH 8, 50 mM BisTris pH 6.0, 0.7 mM TCEP, 6 mM Na azide) was mixed with an equivalent volume of crystallization solution (20% PEG 3350, 20 mM MgCl<sub>2</sub>, 20 M NiCl<sub>2</sub>, 100 mM HEPES pH 7) and equilibrated at room temperature. For PHA7<sub>S</sub>, protein solution (30 mg/mL in 180 mM NaCl, 20 mM sodium phosphate pH 6.5, 5 mM DTT) was mixed with an equivalent volume of crystallization solution (25% glycerol, 2 M (NH<sub>4</sub>)<sub>2</sub>SO<sub>4</sub>) and equilibrated at room temperature. Crystals were frozen without the addition of a cryoprotectant. For PHA7-D175K, 1.5 mM IP(3,4,5)P<sub>3</sub> and protein solution (15 mg/mL in 180 mM NaCl, 20 mM Tris pH 8, 30 mM BisTris pH 6, 0.5 mM TCEP, 6 mM Na azide) were mixed with an equivalent volume of crystallization solution (20% PEG 3350, 200 mM Na acetate) and equilibrated at room temperature. PHA7s crystals appeared in 13 days and grew for an additional 7 days before freezing. PHA7<sub>APO</sub> and PHA7-D175K crystals appeared after 1 day and grew for another 3 days before freezing. Crystals were frozen after addition of glycerol to final concentration 20% v/v.

X-ray diffraction data for PHA7<sub>APO</sub> and PHA7<sub>S</sub> were collected at the Advanced Light Source (Berkeley, CA) beamline 8.3.1, with a wavelength 1.116 Å and temperature of 100 K. The data for PHA7-D175K were collected on a Rigaku diffractometer with R-axis detector, with a wavelength of 1.54 Å and temperature of 100 K. The data were processed using the CCP4 suite (Winn et al., 2011), to resolution of 2.80 Å (PHA7<sub>APO</sub>), 1.45 Å (PHA7<sub>S</sub>) and 2.43 Å (PHA7-D175K). The structure of PHA7<sub>S</sub> was solved first, with molecular replacement guided by the structure of PEPP1 (PDB: 1UPR; 52% identity). Phenix. AutoBuild (Adams et al., 2010) was used for initial model building, followed by several rounds of manual model inspection and correction in Coot (Emsley et al., 2010) and refinement by phenix.refine (Adams et al., 2010) and Refmac5 (Murshudov et al., 2011). The structures of PHA7<sub>APO</sub> and PHA7-D175K were solved with Phaser (McCoy et al., 2007) using the structure of PHA7<sub>S</sub> as molecular replacement model, and refined as for PHA7<sub>S</sub>.

Molprobity (Chen et al., 2010) and the PDB validation server were used for structure validation throughout refinement. All structures had Ramachandran statistics with more than 95% of residues in favored positions and less then 1% outliers. Poisson-Boltzmann electrostatics were calculated in PyMOL 2.2 using APBS (Baker et al., 2001). Illustrations were prepared using PyMol 2.2.

#### **NMR** experiments

NMR experiments were performed with 450 µL samples in NMR buffer, on a Bruker Avance spectrometer, equipped with a Bruker  $^{1}$ H/ $^{15}$ N/ $^{13}$ C triple-resonance cryoprobe, operating at a  $^{1}$ H frequency of 600 MHz. Assignments of the solution NMR resonances from N, HN, CA and CB were obtained using HNCA (Grzesiek and Bax, 1992) and HNCACB (Wittekind and Mueller, 1993) experiments. Chemical shifts were referenced to the  $H_2O$  resonance (Cavanagh et al., 1996). Secondary structure was characterized by analyzing the chemical shifts with TALOS+ (Cornilescu et al., 1999; Shen et al., 2009). The total differences (ΔHN) in amide <sup>1</sup>H and <sup>15</sup>N chemical shifts due to the C-terminus or peptide binding were calculated by adding the changes in  $^{1}$ H ( $\Delta$ H) and  $^{15}$ N ( $\Delta$ N) chemical shifts using the equation  $\Delta$ HN=  $(1/2) [(\Delta H)^2 + (\Delta N/5)^2]$ . The NMR data were processed and analyzed using NMRPipe (Delaglio et al., 1995), Sparky (Goddard and Kneller, 2004) and NMRView (Johnson and Blevins, 1994). The NMR pulse sequences are described in detail in the literature (Bax and Grzesiek, 1993; Cavanagh et al., 1996; Clore and Gronenborn, 1998; Ferentz and Wagner, 2000; Fesik and Zuiderweg, 1990; Kay, 2001).

#### **Molecular dynamics simulations**

All-atom MD simulations were performed using the CHARMM36(m) force fields for protein and lipids (Brooks et al., 2009; Klauda et al., 2010), with the TIP3P water model (Jorgensen et al., 1983) in 100 mM NaCl. All systems were prepared and equilibrated using CHARMM-GUI Solution Builder and Membrane Builder (Jo et al., 2008, 2009; Lee et al., 2019). The temperature and pressure were maintained at 318.15 K and 1 bar. MD production simulations were conducted with OpenMM (Eastman et al., 2013) for 1 μs, and the last 500 ns of trajectories were used for analysis. The initial structural model was taken from the crystal structure of PHA7<sub>S</sub>; all ligands were removed and residues 236-254 were modeled using GalaxyFill, latest version (Ko et al., 2011).

Ten MD simulations were performed for each of the three membrane systems (Table S2), for a total of thirty independent simulations. The initial system size of each replica was 90 Å × 90 Å x 175 Å to accommodate for all initial components, yielding a total of approximately 125,000 atoms per replica. All analyses were performed using CHARMM, and models were visualized with VMD, version 1.9.4 (Humphrey et al., 1996) and PyMOL 2.2 (DeLano, 2002).

#### **QUANTIFICATION AND STATISTICAL ANALYSIS**

The ITC values in Table 1 represent the average of triplicate experiments performed for each ligand.

# **Supplemental Information**

Structural basis for the association of PLEKHA7 with membrane-embedded phosphatidylinositol lipids

Alexander E. Aleshin, Yong Yao, Amer Iftikhar, Andrey A. Bobkov, Jinghua Yu, Gregory Cadwell, Michael G. Klein, Chuqiao Dong, Laurie A. Bankston, Robert C. Liddington, Wonpil Im, Garth Powis, and Francesca M. Marassi

## **Supplementary Information**

# Structural basis for the association of PLEKHA7 with membrane-embedded phosphatidylinositol lipids

Alexander E. Aleshin <sup>1,3</sup>, Yong Yao <sup>1,3</sup>, Amer Iftikhar <sup>2</sup>, Andrey A. Bobkov <sup>1</sup>, Jinghua Yu <sup>1</sup>, Gregory Cadwell <sup>1</sup>, Michael G. Klein <sup>1</sup>, Chuqiao Dong <sup>2</sup>, Laurie A. Bankston <sup>1</sup>, Robert C. Liddington <sup>1</sup>, Wonpil Im <sup>2</sup>, Garth Powis <sup>1</sup>, Francesca M. Marassi <sup>1,\*</sup>

This PDF file includes: Figures S1 to S5

Tables S1 to S2

Cancer Center, Sanford Burnham Prebys Medical Discovery Institute, 10901 North Torrey Pines Road, La Jolla CA, 92037

<sup>&</sup>lt;sup>2</sup> Departments of Biological Sciences, Chemistry, and Bioengineering, Lehigh University, PA 18015, USA

<sup>&</sup>lt;sup>3</sup> Authors contributed equally

<sup>\*</sup> Address correspondence to fmarassi@sbp.edu

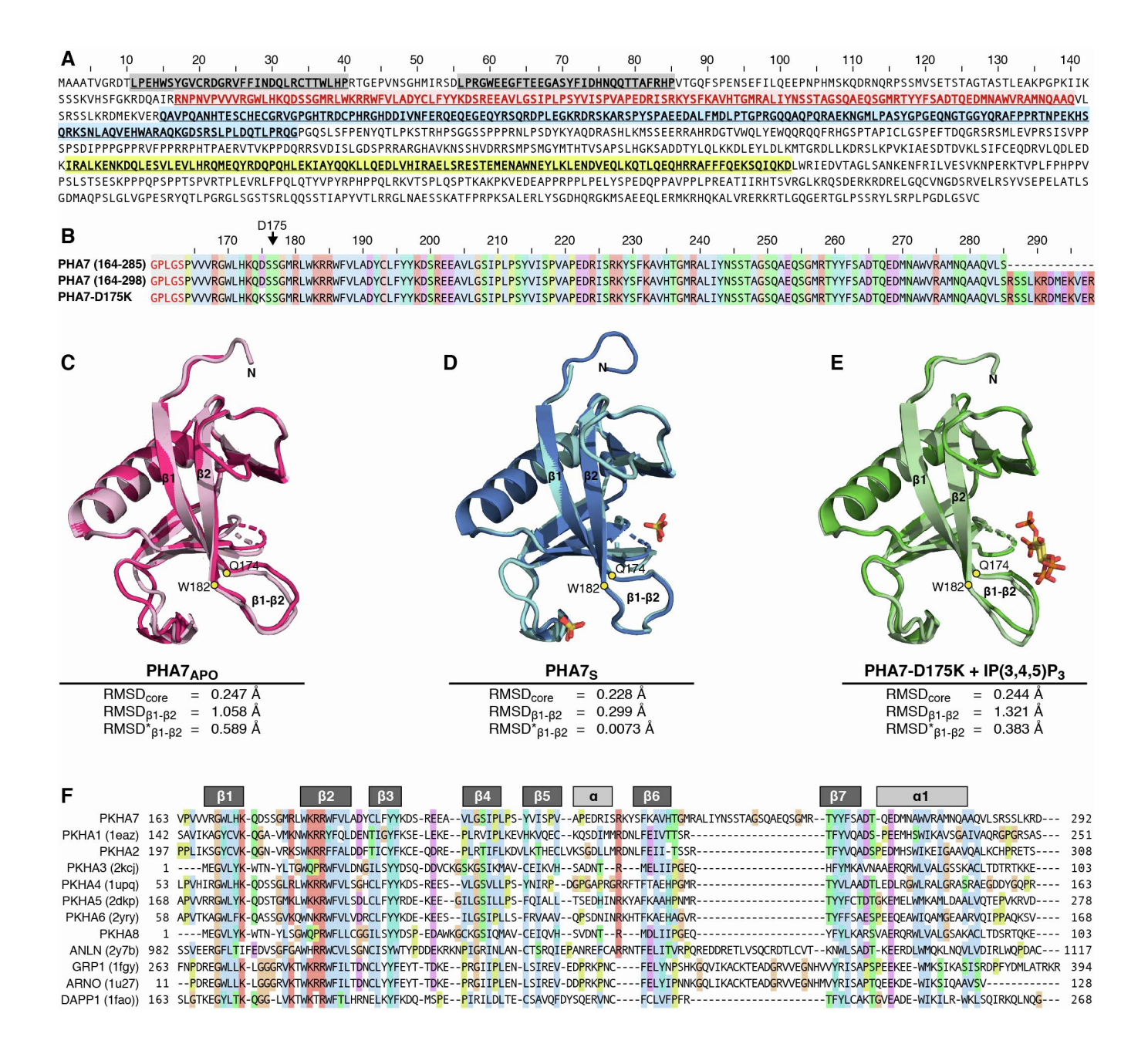


Figure S1. PHA7 sequences and structures (related to Figure 1).

- (A) Amino acid sequence and domain organization of PHA7. Regions with homology to conserved domains are highlighted in colored boxes for: WW domains (gray); PH domain (red), NESP55 (blue); and domains of unknown function (yellow). The WW domain is characterized by two highly conserved Trp that bind proline-rich peptide motifs. NESP55 (neuroendocrine-specific golgi protein P55) is a novel member of the chromogranin family and is a soluble, acidic, heat-stable secretory protein that is expressed exclusively in endocrine and nervous tissues, although less widely than chromogranins. This family consists of several mammalian neuroendocrine-specific golgi protein P55 (NESP55) sequences.
- **(B)** Amino acid sequences of wild-type PHA7 and mutant PHA7-D175K used for structure determination, NMR and ITC studies. The sequence begins at residue P164 after N-terminal cloning artifacts (red font over gray background).
- (C-E) X-ray crystal structures of PHA7<sub>APO</sub> (pink/magenta), PHA7<sub>S</sub> (cyan/blue) and PHA7-D175K (pale green/green). The two copies of the protein resolved for each crystallographic asymmetric unit are superimposed. RMSD<sub>core</sub> is calculated for the best matching CA atoms after alignment of the entire molecule. RMSD $_{\beta1-\beta2}$  is calculated for CA atoms of the  $\beta1-\beta2$  loop (Q174-W182) after alignment of the entire molecule. RMSD $_{\beta1-\beta2}$  is calculated for CA atoms of the  $\beta1-\beta2$  loop after alignment of the  $\beta1-\beta2$  loop. Structures were rendered with Pymol (DeLano, 2002).
- **(F)** Structure-based sequence alignment of PLEKHA family and other PH domains. Alignments were generated and colored with Clustal Omega using Jalview (Clamp et al., 2004, *Bioinformatics* 20: 426). Conserved secondary structure is shown above the sequences. PDB codes are for sequences with deposited three-dimensional structures.

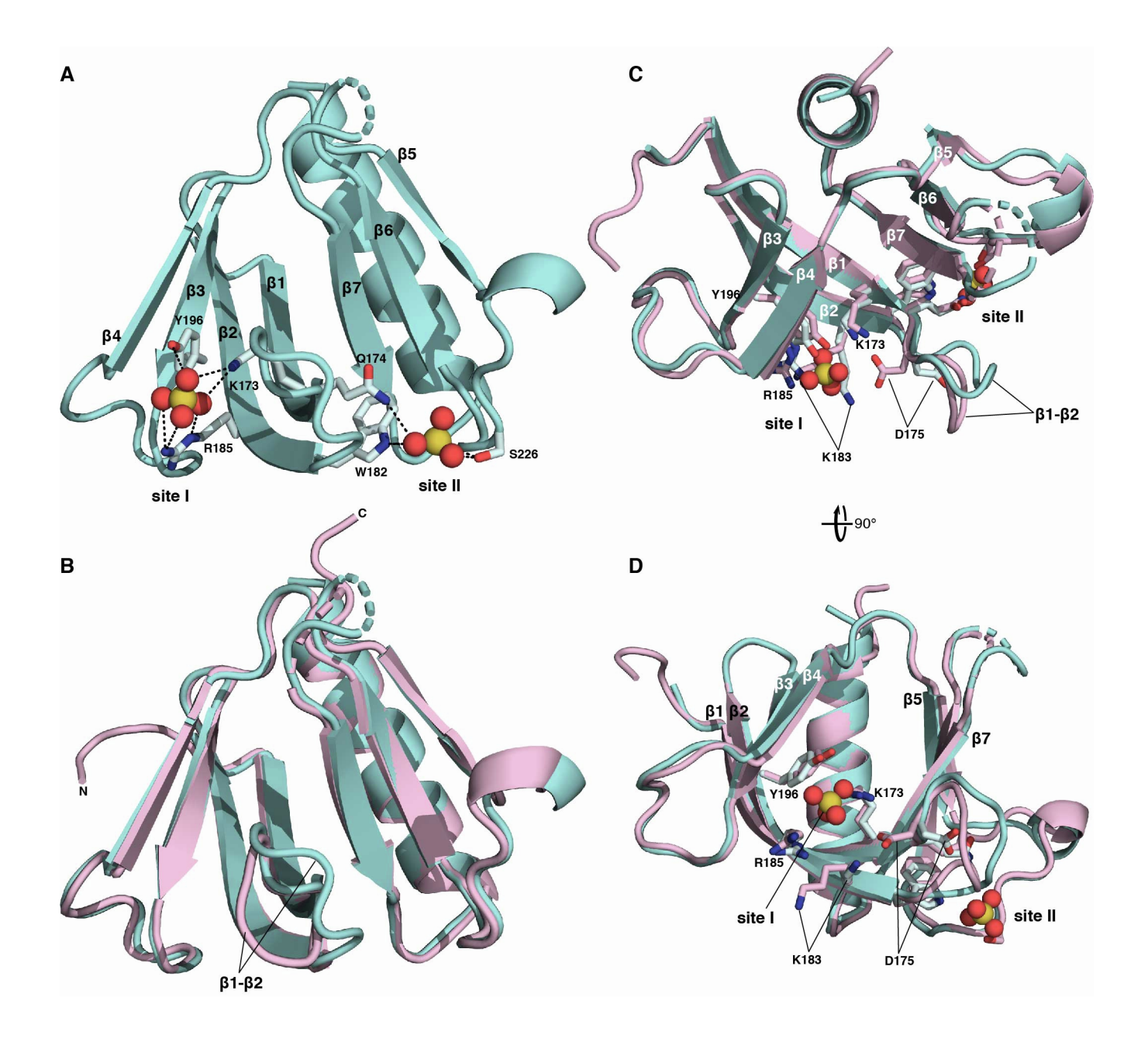


Figure S2. Comparison of the structures of PHA7<sub>APO</sub> (pink) and PHA7<sub>S</sub> (cyan) (related to Figure 1). Sidechains involved in sulfate coordination are shown as sticks. Sulfate anions are shown as spheres (sulfur in yellow; oxygen in red).

- (A) View of the two binding sites (I and II) for sulfate of PHA7s.
- (B) Structural superposition of PHA7<sub>APO</sub> and PHA7<sub>S</sub>. The  $\beta$ 1- $\beta$ 2 loop differs in the two structures.
- (C, D) Orthogonal view of the superimposed structures of PHA7<sub>APO</sub> and PHA7<sub>S</sub>.

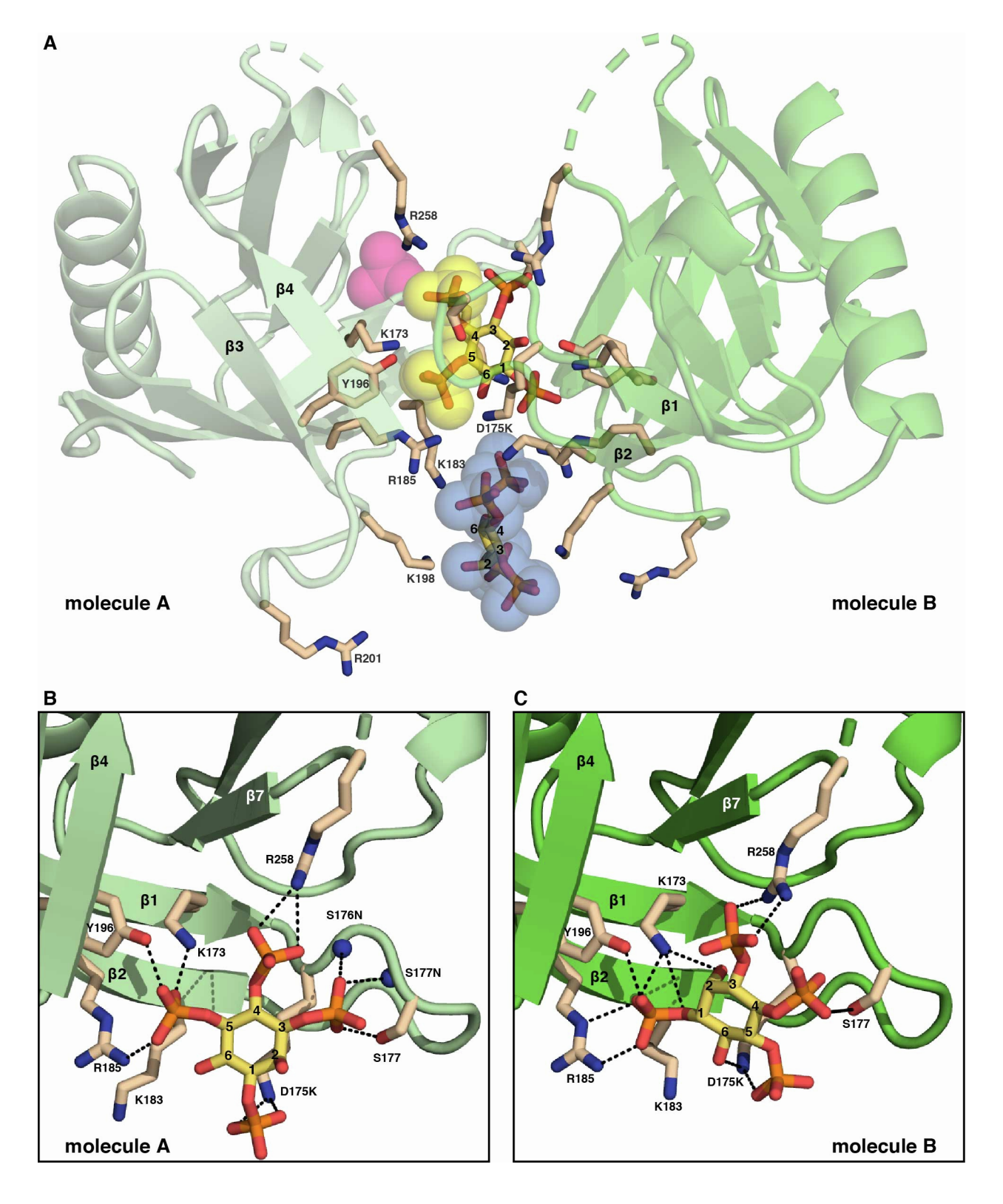


Figure S3. Structure of PHA7-D175K (related to Figure 1).

(A) Two molecules of PHA7-D175K (pale green, dark green) in the crystallographic asymmetric unit coordinate two  $I(1,3,4,5)P_4$  molecules sandwiched between them. One  $IP(3,4,5)P_3$  molecule occupies the principal binding site. The fifth phosphate group on the inositol ring occupies binding site I and coincides with the sulfate anion that binds in the structure of PHA7<sub>S</sub> (cyan). The second  $IP(3,4,5)P_3$  molecule binds more peripherally.

(B, C) Association of IP(3,4,5)P<sub>3</sub> with site I in each of the two PHA7-D175K molecules of the crystallographic asymmetric unit.

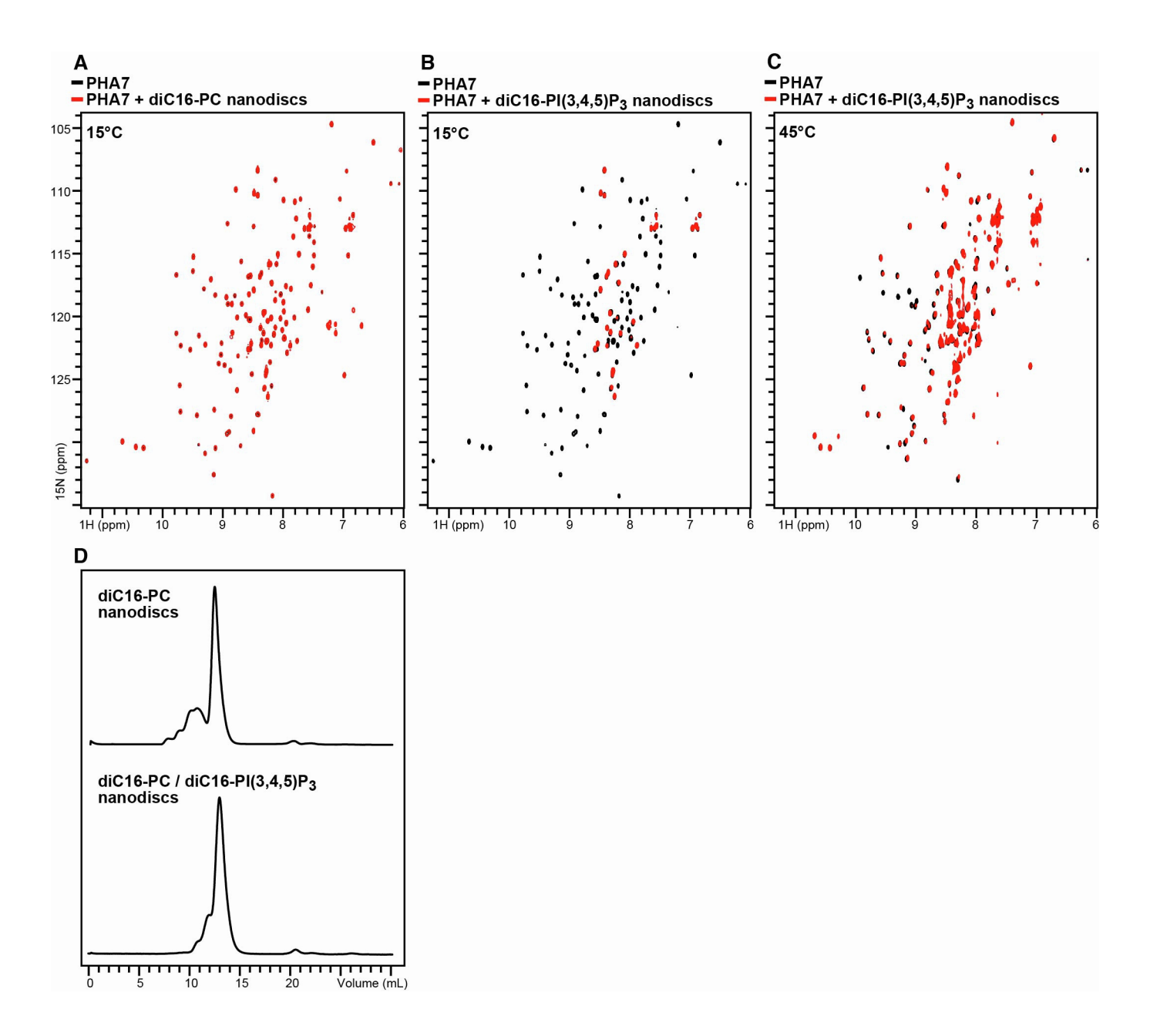


Figure S4. NMR-detected interaction of PHA7 with PIP nanodiscs (related to Figure 4).

(A-C) <sup>1</sup>H/<sup>15</sup>N spectra NMR of <sup>15</sup>N-labeled PHA7 were obtained before (black) or after (red) addition of 1.5 molar equivalents of lipid nanodisc, containing: (A) 100% diC16-PC or (B, C) 10% diC16-PI(3,4,5)P<sub>3</sub>. The spectra were acquired at 15°C (A, B) or 45°C (C)

(D) Size exclusion chromatography elution profile of nanodiscs used in this study. The major peak was collected for NMR experiments.

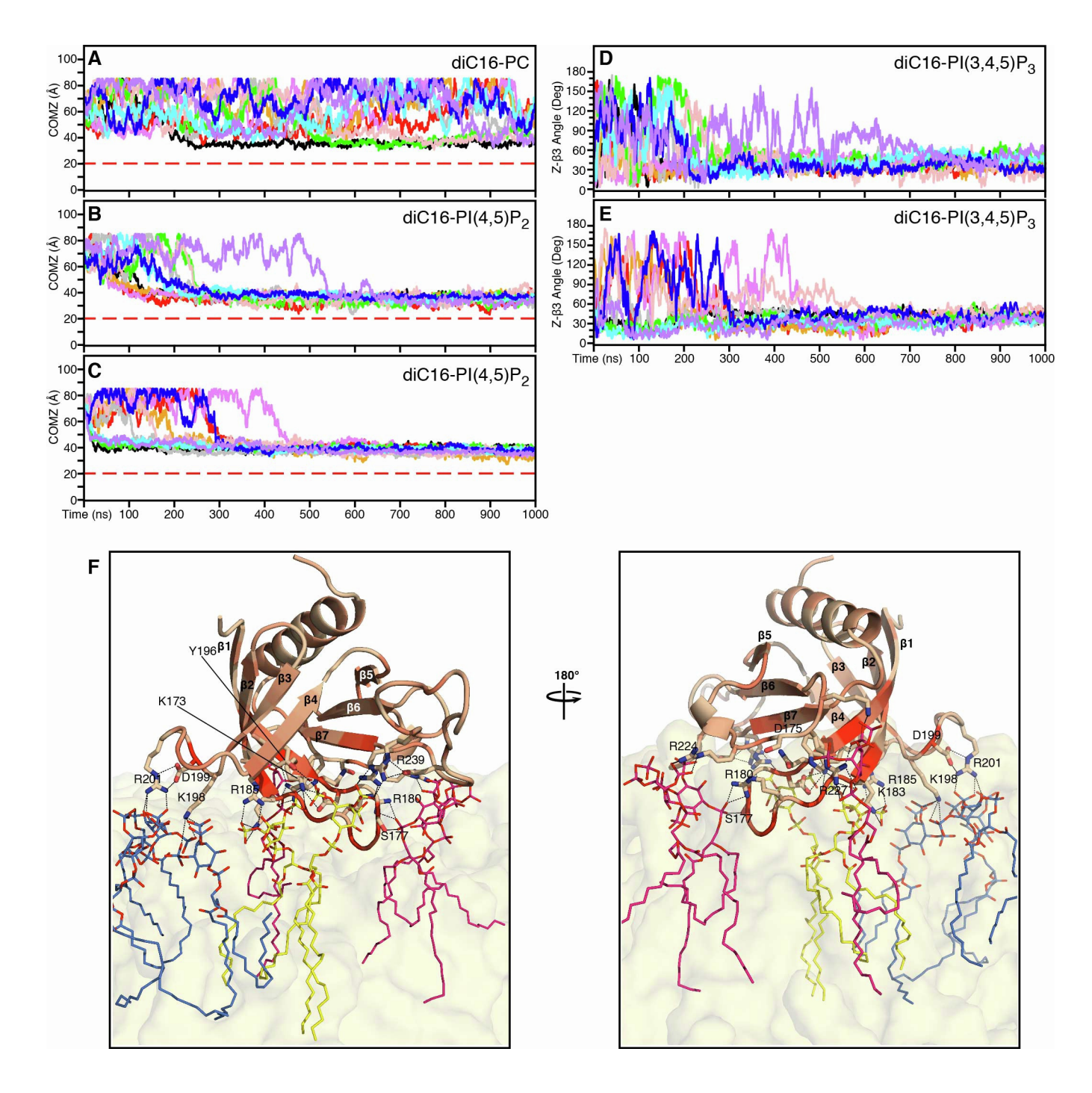


Figure S5. MD simulations for PHA7 association with the membrane surface (related to Figure 5).

(A-C) Time series of the average distance of the center of mass from the center of the lipid bilayer membrane. The distance is measured parallel to the lipid bilayer normal (Z axis) with the lipid bilayer center at Z = 0 Å. The average location of the lipid head groups is at Z = 20 Å (dashed red line). Different colors represent each of 10 independent simulations of PHA7 in: (A) pure diC16-PC membranes; (B) membranes containing 10% diC16-Pl(4,5)P<sub>2</sub>; or (C) membranes containing 10% diC16-Pl(3,4,5)P<sub>3</sub>. Through the periodic boundary conditions, PHA7 can associate with the lower bilayer leaflet (near Z = 85 Å). While PHA7 shows no specific binding to PC-only membranes, simulations with either Pl(4,5)P<sub>2</sub> or Pl(3,4,5)P<sub>3</sub> resulted in protein association with the membrane surface.

(**D**, **E**) Time series of the average preferred orientation on PIP membranes. Different colors represent each of 10 independent simulations for membranes containing 10% diC16-PI(4,5)P<sub>2</sub> (D) or 10% diC16-PI(3,4,5)P<sub>3</sub> (E).

**(F)** PIP clustering induced by PHA7 association with the membrane surface. Snapshot (taken at 890 ns) of MD simulation of PHA7 with a diC16-PI(3,4,5)P<sub>3</sub> membrane. PHA7 colors reflect the magnitude of NMR chemical shift perturbation from 0 ppm (wheat) to the maximum value (red). Key side chains with close (< 4 Å) contacts to PIP headgroups are shown as sticks. The membrane is represented as a molecular surface (yellow). Colors of bound PIP molecules (lines) represent their association with binding sites I (yellow), II (pink), or III (blue).

Table S1. Data collection and refinement statistics (molecular replacement) a, b. Related to Figure 1.

		PHA7 <sub>APO</sub> (PDB: 7kk7)	PHA7 <sub>s</sub> PDB: 7kjo)	PHA7-D175K (PDB: 7kjz)
Data collect	ion			
Space group		P 2 <sub>1</sub> 2 <sub>1</sub> 2 <sub>1</sub>	P 4 <sub>1</sub>	P 3 <sub>2</sub> 2 1
Cell dimens	ions			
	a, b, c (Å)	57.31 59.06 78.47	64.83 64.83 59.23	77.47 77.47 82.56
	α, β, γ (°)	90 90 90	90 90 90	90 90 120
Resolution (	Å) (outer shell)	47.2 -2.80 (2.95 -2.80)	43.7-1.45 (1.48-1.45)	52.1-2.43 (2.53-2.43)
No. reflection		6980 (1000)	46929 (4283)	11134 (1136)
Wavelength	(Å)	1.116	1.116	1.54
$R_{\text{merge}}$		0.071 (0.81)	0.050 (0.362)	0.058 (0.56)
1/σΪ		16.0 (2.5)	22.2 (2.30)	21.8 (3.9)
CC <sub>1/2</sub>		0.99 (0.89)	n/d	0.99 (0.91)
Completene	ess (%)	100.0 (100.0)	99.2 (99.0)	99.9 (99.9)
Redundanc	y	6.8 (7.1)	19.0 (18.1)	10.4 (9.9)
Refinement			45.84 –1.45	38.8 - 2.43
Resolution (	Å)	47.2 – 2.80	43487 / 2187	10443 / 668
No. reflection		6595 / 453	0.155 / 0.171	0.201 / 0.236
Rwork / Rfree		0.212 / 0.276		
No. atoms			1940	1794
	Overall	1701	1695	1672
	Protein	1671	38	66
	Ligand/ion	22	207	60
	Water	8		
B-factors		400.0	29.3	71.3
	Overall	100.0	27.4	70.2
	Protein	100.0	51.9	112.5
	Ligand/ion	106.1	39.9	56.9
	Water	75.8	0.000	0.040
R.M.S. devi		0.011	0.023	0.013 1.72
	Bond lengths (Å)	0.011 1.78	1.78 97.5 / 0.0	97.4 / 0.0
Б	Bond angles (deg)	96.9 / 0.5	91.0/0.0	91.4/0.0
Ramachand	Iran favored/outliers (%)	90.9 / 0.3		

Table S2. Lipid compositions of each system generated for MD simulations (related to Figure 5).

Membrane system	Number of lipid molecules per membrane system			
Membrane system	diC16-PC	diC16-PI(4,5)P <sub>2</sub>	diC16-PI(3,4,5)P <sub>3</sub>	
PHA7 + PC	120	0	0	
PHA7 + PI(4,5)P <sub>2</sub>	108	12	0	
PHA7 + diC16-PI(3,4,5)P <sub>3</sub>	108	0	12	

<sup>&</sup>lt;sup>a</sup> Each data set was collected from a single crystal. <sup>b</sup> Values in parentheses are for the highest-resolution shell.